npj | Climate and Atmospheric Science

www.nature.com/npjclimatsci

REVIEW ARTICLE OPEN

Check for updates

Lifecycle of light-absorbing carbonaceous aerosols in the atmosphere

Dantong Liu[1]✉, Cenlin He[2], Joshua P. Schwarz[3] and Xuan Wang[4]

Light-absorbing carbonaceous aerosols (LACs), including black carbon and light-absorbing organic carbon (brown carbon, BrC), have an important role in the Earth system via heating the atmosphere, dimming the surface, modifying the dynamics, reducing snow/ice albedo, and exerting positive radiative forcing. The lifecycle of LACs, from emission to atmospheric evolution further to deposition, is key to their overall climate impacts and uncertainties in determining their hygroscopic and optical properties, atmospheric burden, interactions with clouds, and deposition on the snowpack. At present, direct observations constraining some key processes during the lifecycle of LACs (e.g., interactions between LACs and hydrometeors) are rather limited. Large inconsistencies between directly measured LAC properties and those used for model evaluations also exist. Modern models are starting to incorporate detailed aerosol microphysics to evaluate transformation rates of water solubility, chemical composition, optical properties, and phases of LACs, which have shown improved model performance. However, process-level understanding and modeling are still poor particularly for BrC, and yet to be sufficiently assessed due to lack of global-scale direct measurements. Appropriate treatments of size- and composition-resolved processes that influence both LAC microphysics and aerosol–cloud interactions are expected to advance the quantification of aerosol light absorption and climate impacts in the Earth system. This review summarizes recent advances and up-to-date knowledge on key processes during the lifecycle of LACs, highlighting the essential issues where measurements and modeling need improvement.

npj Climate and Atmospheric Science (2020)3:40 ; https://doi.org/10.1038/s41612-020-00145-8

INTRODUCTION

Light-absorbing carbonaceous aerosols (LACs) is one of the most important radiatively-active components in the Earth system. They absorb sunlight, reduce snow/ice albedo, and introduce positive radiative effects. LACs consist of black carbon (BC) and absorbing organic aerosol (brown carbon, BrC), which are ubiquitous from both natural and anthropogenic emissions. LACs exist mostly in sub-micron sizes, and can efficiently absorb solar radiation from the near ultraviolet (UV) throughout the visible and to the near-infrared (IR) wavelengths, perturbing the energy balance of the climate system in important ways. LACs undergo complex transformations during their lifecycle in the atmosphere including emission, evolution, transport, and removal, which determine LAC lifetime, destination, and climate impact. Several nice reviews in the past decade about light absorption of LACs[1], climatic impacts of BC[2], and chemistry of BrC[3] are available. This paper aims to summarize recent scientific advance and up-to-date knowledge of key processes and consequent impacts of LACs during their atmospheric lifecycle, highlight uncertainties associated with each process, and suggest future directions in reducing the uncertainties in constraining the impacts.

This review is arranged into the main sections of (1) emission and source profile of LACs (basic physiochemical properties and the measurement techniques in characterizing LACs), (2) transport (vertical, horizontal, and high-altitude transport), (3) evolution and transformation (ageing processes of LACs), and (4) removal from the atmosphere (in-cloud and below-cloud scavenging, dry deposition, and deposition in the cryosphere).

Some key quantities are often used in assessing LAC composition and impacts. The LAC ability to absorb light is commonly represented using the mass absorption cross-section (MAC; absorption cross-section per unit mass with a unit of $m^2\ g^{-1}$). The wavelength (λ) dependence of absorption can be expressed using the absorption Ångström exponent (AAE) in a power-law relationship,

$$\mathrm{MAC}(\lambda) = A \cdot \lambda^{-\mathrm{AAE}}, \quad (1)$$

where A is the scaling factor dependent on aerosol composition and size distribution. A higher AAE means a more efficient absorption at a shorter wavelength. Both MAC and AAE are determined by the distribution of chromophores in the molecular structure of species. BC contains mostly sp^2-bonded graphite layer and absorbs throughout the near-UV to near-IR spectrum with AAE ~1[4]. BrC absorbs mainly at near-UV but is almost transparent at the red-yellow wavelengths, thus with brownish appearance[5].

The factors influencing the direct radiative forcing (DRF) of LACs can be decomposed as[6],

$$\mathrm{DRF} = E \times L \times \mathrm{MAC} \times \mathrm{AFE}, \quad (2)$$

where E is the emission rate, L is the lifetime, and AFE is the absorption forcing efficiency (per unit of column absorption optical depth), a catch-all that includes any other factors that influence the radiative forcing. The discussion below will mirror the terms in Eq. 2, and provide context on the emission, transport, evolution (aging), and removal (deposition) of LACs as illustrated in Figs. 1 and 2.

Another important quantity is the modified combustion efficiency (MCE), which is often used as a measure of the burning phase or combustion conditions. MCE is defined as the net emitted CO_2 from the sources (relative to background) over the

[1]Department of Atmospheric Sciences, School of Earth Sciences, Zhejiang University, Hangzhou, China. [2]Research Applications Laboratory, National Center for Atmospheric Research, Boulder, CO, USA. [3]Chemical Sciences Division, Earth System Research Laboratory, National Oceanic and Atmospheric Administration Boulder, Boulder, CO, USA. [4]School of Energy and Environment, City University of Hong Kong, Hong Kong SAR, China. ✉email: dantongliu@zju.edu.cn

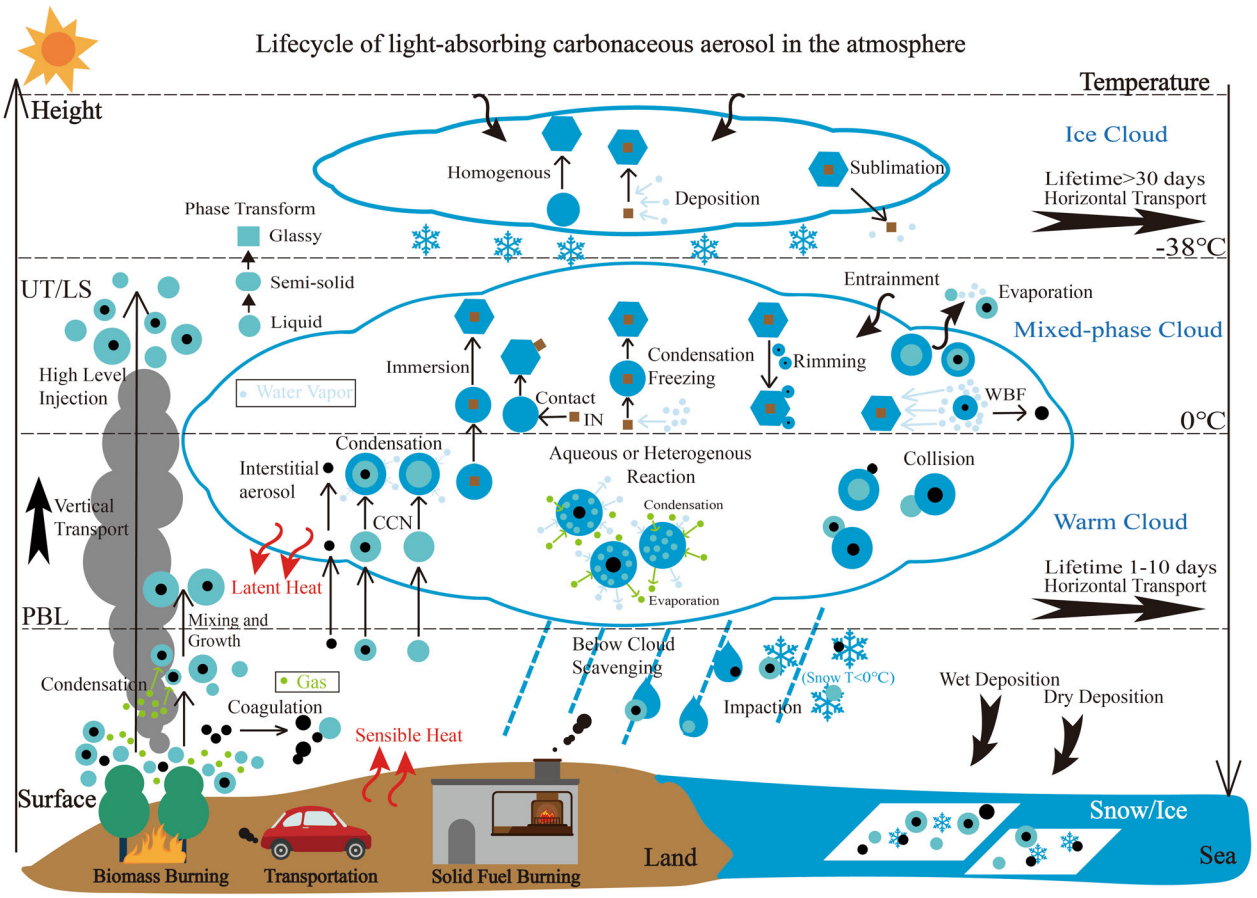

Fig. 1 Schematic overview of the key processes during the lifecycle of light-absorbing carbonaceous aerosols (LACs) in the atmosphere. The processes are demonstrated as the occurrence at different atmospheric layers, in or out of cloud. The arrows indicate the direction of processes or the transport of substances.

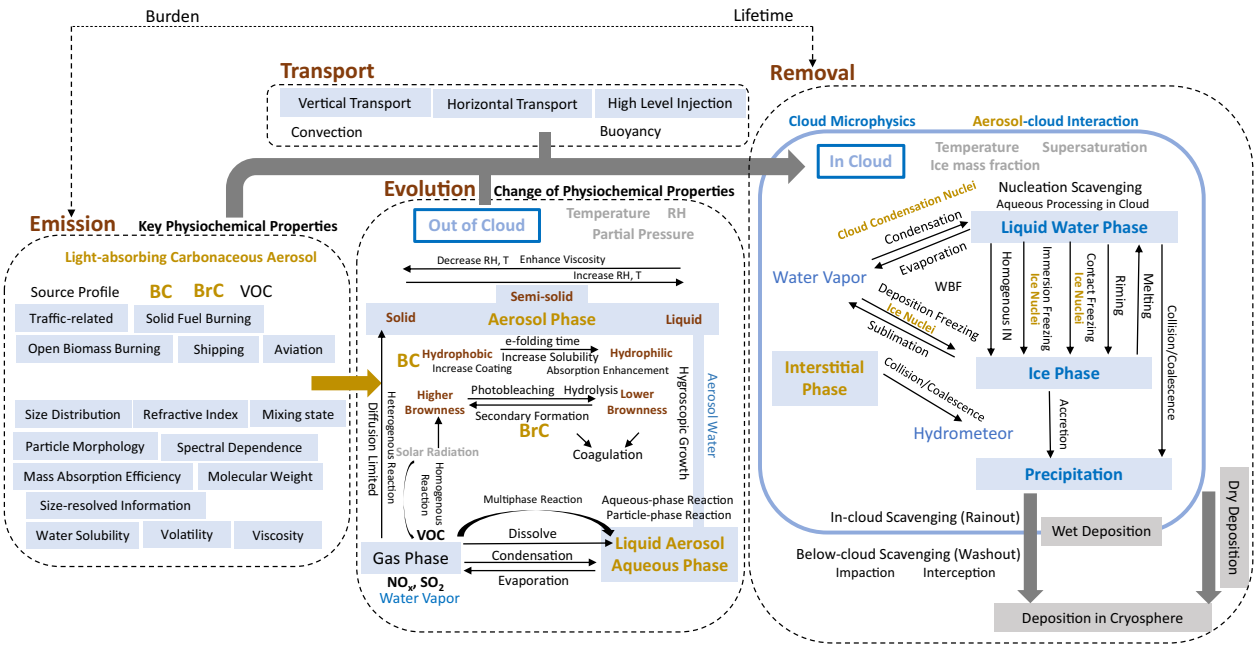

Fig. 2 Flow diagram of detailed atmospheric processes on LACs during their lifetime. The processes from emission, transport and evolution to the removal from the atmosphere, are shown in separate blocks.

total net emitted carbon oxide ($CO_2 + CO$)[7]. A higher MCE (typically > 0.95)[8,9] denotes the high-temperature flaming phase, while a lower MCE is associated with smoldering, less efficient burning.

EMISSIONS AND SOURCE PROFILES OF LACs

BC and BrC are emitted from a range of anthropogenic and natural combustion sources, but their properties could be modified after emissions. BrC also has secondary non-combustion sources that is currently believed to be mostly associated with nitrogen chemistry[3]. The physiochemical properties of all types of LACs are summarized in Table 1.

Physiochemical properties

The fundamental physiochemical properties of BC has been comprehensively summarized by Bond et al.[2], which include the strong absorption at all visible wavelengths with a MAC of >5 m^2 g^{-1} in the green, refractory with vaporization temperature near 4000 K, containing sp^2-bonded graphite layers, aggregate morphology (Table 1), and being chemically stable and insoluble in water or common organic solvents. The strong chemical stability and primary-only sources of BC mean that under many occasions it can serve as an ideal tracer to track aerosol emission sources and atmospheric scavenging processes.

Most organic compounds are transparent in the visible and near-IR, while BrC contains chromophores that absorb in the near-UV ($\lambda = 300$–400 nm) but substantially less so in the yellow-red band. Figure 3 gives the spectral imaginary refractive indices of all LAC types (BC and BrC with a range of absorptivity) as mostly used in models. BrC usually contains compounds with polycyclic rings or aromatics associated with nitrated, carbonyl, and unsaturated function groups. BrC has a range of volatility, while the substances with higher molecular weight (MW) and low volatility tend to have stronger absorptivity[3]. A conventional proxy for BrC is the atmospheric humic-like substances (HULIS), which contains polycyclic ring structures with a range of unsaturated hydrocarbon side chains[5]. HULIS could be from primary emissions of biomass burning after aqueous processing[10] and also take up secondary species from biogenic and anthropogenic sources[11].

Tar balls, which are typically spherical in shape and quite viscous, unlike both BC and other BrC, are often observed from biomass smoldering smoke. They are composed of organic compounds with extremely low volatility that can survive in the vacuum environment of transmission electron microscopy (TEM) beam[12]. Tar balls are largely homogeneous in composition and contain a modest degree (similar to HULIS) of sp^2 hybridization[13]. They have highly uncertain imaginary refractive indices, even estimated to reach values comparable to that of BC, throughout the absorption spectrum[14].

Emission profiles

A large range of co-emitted species can be either instantaneously mixed with LACs soon after emission, or during transport in the atmosphere (see "Transport of LACs" section). These substances can become mixed with LACs via vapor condensation or particle coagulation. This indicates that at the single particle or population level, multiple components can co-exist.

Non-traffic burning sources usually generate BC associated with more non-BC materials contained in individual particles (coatings on BC, without suggesting knowledge of the physical arrangement of the various components), while BC from diesel engines can typically be referred to as near-pure BC[15,16]. The MCE importantly determines the OA/BC ratio. The smoldering phase can generate a much higher fraction of organics than BC[17], thus BC in smoldering is more coated with internally mixed organics[9]. Ideally, the burning phases and duration should be parameterized to more realistically represent these conditions[6,18]. It is clear that the physiochemical properties of BC, such as the initial size, optical properties, and hygroscopicity, from different sources or under different combustion conditions should be treated differently.

Mixing of BC and BrC can also be significant. Primary biomass-burning sources usually co-emit BrC with BC[5], while the traffic-related sources tend to emit purer BC without significant organics[19]. The optical properties of a mixture of BC and BrC depend on the relative contribution of each constituent to optics. A higher BrC optical fraction will cause more absorption at shorter wavelengths, i.e., a larger AAE, than that dominated by BC. Saleh et al.[20] find that the absorptivity of BrC (MAC or imaginary refractive index k) is larger during high-temperature combustion when co-emitted with BC, and these BrC species have low volatility and high molecular weight (MW), whereas BrC from smoldering phase burning has a lower MAC. In addition, an inverse correlation was found between k and AAE[21], with weak absorption efficiencies corresponding to absorption mainly in the UV but not in the visible. The information could be consistently correlated with a BC/OC ratio, which has been used to parametrize the BrC optical properties based on emission inventories[22,23]. Similarly, this leads to the widely used technique of using the spectral dependence of absorbance to separate open-burning and traffic sources[24].

In general, fresh BC particles near sources typically have primary spherule or monomer diameter of 10–50 nm, with fractal dimensions of typically 1.5–2.2 (3 is for a void-free sphere)[25,26]. Studies measuring the refractory BC component in BC-containing particles (termed the BC core) showed larger mass-median diameter BC core size generated from open biomass burning[15] and residential solid fuel burning[27], and ~20–30 nm smaller mass-median diameter cores from diesel emission. However, number-median diameter may be uncertain if even smaller BC cores were present, such as from gasoline[28]. The BC core size contrast with different sources, in addition to differences in the amount of non-BC material associated with the cores, means the initial optical and hygroscopic properties can be very different even at emission. Such information has been widely configured in models, using different size distributions between biomass burning and transportation sources (see "Modeling on BC aging" section). The size distribution of BrC could be obtained for a specified type such as tar ball through microscopy[29], however, there is currently no definitely defined size distribution for other species of BrC, given their both primary and secondary characteristics.

Emissions from aviation and shipping represent minor contributions to BC mass at the global scale[2], but they occur in either high altitudes or remote regions that are climatically sensitive. Lack et al.[30] found that the emission profile of carbonaceous aerosols from marine shipping depends on the engine size and combustion efficiency, which could be overall correlated with the regular operation speed of vessels, where engines in slow and medium-high speed tend to emit significant BC and OM, respectively. Corbin et al.[31] found that the BrC in the form of highly absorbing tar balls may dominate total aerosol light absorption of ship emissions in the open ocean and Arctic, where the heavy fuel oil was usually used for marine shipping.

Measurement techniques in characterizing LACs

A range of measurement techniques for characterizing LACs is available[32]. Indirect characterizations of LAC use techniques that are unable to directly discriminate BC and BrC but quantify the bulk thermal or optical properties of LAC to allow BC–BrC discrimination. In this case, a range of filter-based offline or semi-online methods is used.

A widely applied technique derives aerosol absorption from the measured light transmission through a loaded filter[33,34], which is used in commercial instruments such as the Particle Soot

Table 1. Summary of the physiochemical properties of LACs.

LAC type	Black carbon (BC)	Brown carbon (BrC)		
		Highly absorbing BrC	Moderately absorbing BrC	Weakly absorbing BrC
Common present forms or other names	Soot, elemental carbon (EC), involatile carbon	Tar ball (in continuous state)	Atmospheric humic-like substances (HULIS, in continuous state)	Water-soluble BrC
Sources (formation mechanism)	High-temperature combustion (flame synthesis of PAHs)	More absorbing BrC from flaming biomass or solid fuel burning than lower-temperature smoldering combustion (pyrolysis and near-source condensation, oxidation, functionization after emission)		Some primary OA after photobleaching; some secondary OA from VOC condensation
Carbon bonding	sp^2 dominated	A range of sp^2/sp^3	Moderate sp^2/sp^3	Low sp^2
Composition	Graphite layers	Chromophores, e.g., aromatics associated with nitrated, carbonyl, and unsaturated function groups		Chromophores being decomposed or newly formed
Morphology				
Shape and particle size	Aggregates of monomers in diameter 10–50 nm, overall diameter 80–220 nm	Sphere mainly at accumulation mode in diameters of hundreds of nanometers; or as coatings		Secondary species, size depending on the condensed substrate
Volatility (vaporization temperature)	Refractory (~4000 K)	Extremely low volatility (~1000 K)	Low to medium volatile	Semi-volatile
Viscosity	Solid	Amorphous solid	Amorphous, semi-solid or liquid depending on temperate and RH	Mostly liquid
Optical properties				
Imaginary refractive index[a]	Weak spectral dependence ~0.7–0.8	~0.3–0.5, slightly enhanced near-UV, also near-IR	In the order of 0.01–0.1, mainly near-UV	In the order of 0.001–0.01, only near-UV
Absorption Ångström exponent (AAE)	AAE ~1	AAE slightly >1	Moderate AAE 2–4	High AAE ~3–8
Hygroscopic properties				
Solubility	Insoluble to any solvents	Mostly insoluble	Partly soluble (usually more in organic solvents)	Soluble
Cloud condensation nuclei	Hard CCN; enhanced CCN after aging	Barely CCN but may enhance through oxidation		More CCN
Ice nuclei	Maybe deposition IN	Maybe deposition/immersion IN when glassy-solid/semi-solid		Hard IN
Atmospheric evolution	Chemically inert; more compact shape after aging, possible absorption enhancement	Chemically unstable; subject to photolysis/photooxidation degradation; may enhance absorption by NO_3 oxidation or ammonia uptake		

[a]Only values for most model applications (shown in Fig. 3) are given.

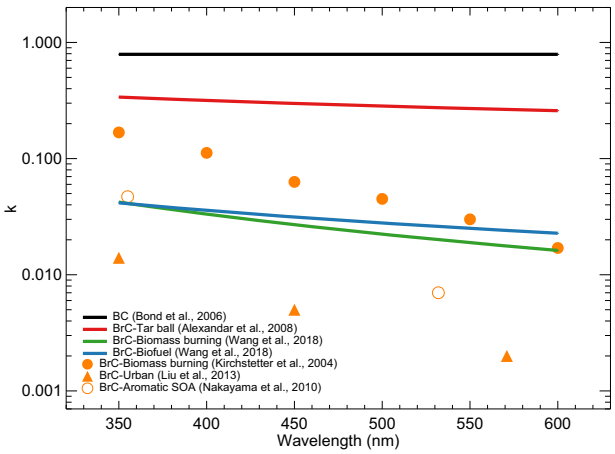

Fig. 3 Summary of the spectral dependence of the imaginary refractive index, *k*. Values from Wang et al.[114] are based on BC/OC parametrization of Saleh et al.[20]. Other values for BrC are selected from measurements and represent the most frequent use in modeling studies (Table 2).

Absorption Photometer (PSAP, Radience Research), the Aethalometer (Magee Scientific), the Tricolor Absorption Photometer (TAP, Brechtel Manufacturing), and the Multi-Angle Absorption Photometer (MAAP, ThermoScientific, Inc.). This technique requires extensive corrections for aerosol accumulation effects, sensitivities to aerosol light scattering, and filter matrix effects on the light field interacting with the particles (which may result in absorption overestimation)[35]. The filter-based absorption measurements are thus subject to corrections that may vary according to the initial mixing between BC and organics, which could lead to considerable uncertainties[36]. A strength of this approach is the ability to quantify light absorption, a typical climate-relevant parameter for LAC.

To chemically speciate BC and OC via thermal decomposition, thermal-optical techniques are used[37] to sequentially volatilize organics at low temperatures and oxidize the remaining refractory BC at high temperatures. In these cases, aerosols are collected on a filter, and then are processed in a temperature-controlled chamber, with the quantification of CO_2 to indicate the amounts of OC or BC evolved throughout the process. Various protocols exist including the timing, temperature plateaus, concurrent detection of transmitted or reflected light (potentially at multiple angles[38]) from the filters, and timing of changing from inert to oxidizing atmosphere[39]. Uncertainties for this technique arise from different protocols, and systematics such as possible pyrolysis of OC (i.e., heated and converted to elemental carbon, EC) causing overestimates of EC, which may be corrected in part by monitoring the optical reflectance or light transmission of the sample filter[40].

A technique with no inherent dependence on filter properties is based on the detection of energy transfer to air from aerosol light absorption. This can be done with a photoacoustic spectrometer (PAS)[41], which measures the standing acoustic wave caused by the pressure change from periodic heating of the aerosol by a laser, or with a photothermal interferometer (PTI)[42], which quantifies the change in air density due to the heating. Careful calibration and removal of gas absorbers are required to obtain the absorption properties of aerosols alone. Additionally, these techniques can only be performed on dry aerosols. PTI and PAS can be applied to multiple wavelengths to quantify AAE. A hyperspectral PAS measurement capability exists[43], but most field-deployed instruments only use three or fewer wavelengths. They may also measure thermally denuded aerosols in addition to dried aerosols[44]. Indirect measurements of absorption have also been achieved by simultaneous measurements of extinction and scattering using cavity-ringdown and integrating nephelometry, respectively[45]. The separation between BC and BrC using an overlapped short wavelength range is challenging as it depends on the assumed mixing state of the morphology of BC[46]. Recent studies have found that low-volatility BrC can absorb at full visible spectrum[31], which raises questions about possible BrC contribution to the optical-thermally characterized EC[47].

A close corollary to EC is refractory BC (rBC)[48], a material detected via the laser-induced incandescence (LII). The LII using pulse laser was conventionally utilized to measure the bulk mass of rBC in relatively high concentration[49]. The application of continuous laser in a cavity for LII was deployed to measure atmospheric rBC[50], which has been further developed to have high sensitivity and become a widely used single-particle measurement in recent decades (the single-particle soot photometer, SP2, DMT Inc.)[51–53]. This direct quantification of rBC concentration for atmospheric measurements was experimentally proved to be equivalent to the optical-thermally determined EC concentration at the 10% level[54]. This technique allows rBC-containing particles to absorb energy from an infrared laser, resulting in heating and associated incandescence with visible light. Both incandescence and scattering signals in single-particle are recorded in the SP2, with the former proportional to the rBC mass[55] and the latter used to derive the mixing state of rBC[56]. This technique is capable of sensitively measuring the mass of an individual rBC-containing particle, as rBC generates a thermal visible light signal that has a unique spectral distribution compared to other refractory aerosol compositions. Although the SP2 provides rBC size distribution information (it is almost always log-normally distributed in mass), it is unable to fully detect very small rBC (diameter < 60 nm) that may contribute strongly to rBC particle number[57]. This technique has also been applied to quantifying rBC in snow, ice, and rainwater[58,59]. A related technique couples the LII with the mass spectrometry to firstly rapidly volatilize rBC-containing particles, the vapors being charged by electron ionization and further detected by mass spectrometry (the soot particle aerosol mass spectrometer, SP-AMS, Aerodyne Inc., MA)[60]. In this way, the composition of internally mixed materials containing rBC can be determined.

TRANSPORT OF LACs

Vertical transport and advection

The vertical transport and advection of pollution are typically governed by local-to-large scale air motions influenced by frontal boundaries, convective cells, and mesoscale/global-scale circulation. LAC-specific effects on transport mainly arise from atmospheric heating induced by light absorption. The heating, depending on the location of the heated layer in the column, could result in the self-lofting of LAC-polluted air masses or the stabilization of light-absorbing layers against mixing[61]. When heating occurs at lower altitude levels, it can promote vertical instabilities that enhance convection above the heating layer; or the opposite can occur when heating at higher levels, resulting in the stabilization of the column below and depressing the vertical mixing. The heating effect, acting over the height of LAC-concentrated layers, can inhibit vertical dispersion of the layers and may enhance their long-range transport[61]. This is also related to the semi-direct impacts of LAC heating layers in modifying the cloud dynamics in either promoting convection or inhibiting the vertical development of clouds[62].

Observations have shown that BC can be efficiently transported to the top of the planetary boundary layer (PBL)[63], generating strong solar absorption at the top of polluted PBL[64–66] and leading to potential feedbacks in trapping pollutants in the PBL[67]. The direct forcing efficiency of BC is considerably enhanced if the

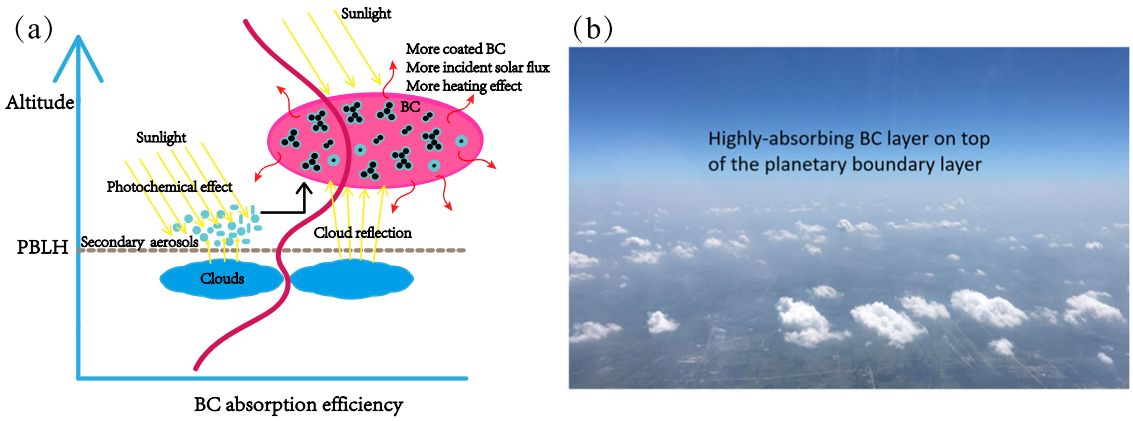

Fig. 4 BC forcing efficiency above cloud. Field observation of enhanced forcing efficiency of BC above the cloud layer over megacities in summertime (**a** schematics and **b** images), resulting from the combined effects of enhanced secondary formation, BC coatings and cloud reflection above the PBL. (Reprinted with permission from ref. [65]. Copyright 2019 IOP Publishing).

underlying layer is highly reflective, such as over cloud layers or snow surface[68] or when at high altitudes with enhanced net actinic fluxes[69]. A recent aircraft observation[65] showed enhanced coating formation on BC above the cloud layer over the top of the urban PBL during summer time (Fig. 4), which greatly increases BC forcing efficiency through the combined effects of cloud reflection and enhanced BC absorption from the coating.

High-altitude transport

Open biomass burning (e.g., wildfires) generates a buoyant heated smoke plume, hence the smoke plume can rise above the well-mixed PBL into the troposphere, and potentially even into the lower stratosphere if it can trigger a pyrocumulonimbus (PyroCb) convective cell. The approximate direct injection height of primary emissions is one of the largest uncertainties influencing modeling of open biomass-burning smoke and is presently estimated in global-scale models via a parameterization of fire radiative power (measured by satellite) to plume rise[70].

The smoke transported higher in the troposphere will experience less possibilities to be removed by wet or dry deposition, hence can have an extended lifetime and longer-range transport, exerting larger climate impacts. Although the initial injection processes affect all aerosols and gases, the post-lofting of pollution due to localized heating of air masses is specifically associated with light-absorbing materials (both gas and aerosol phases). Yu et al.[71] found that the wildfire plume from western Canadian rose from 12 to 23 kilometers owing to solar heating of LACs with extended lifetime and spatial distribution. Considerable loadings of BrC were also observed over continental NA between 5 and 12 km[72], which was speculated to be transported through deep convection while cloud processing may produce secondary BrC along with the vertical transport.

The heating of LACs persisting in the upper troposphere/lower stratosphere (UT/LS) could introduce stronger positive radiative forcing at the top of the atmosphere compared to heating layers present in the lower level[69]. GCM climate models suggest that BC heating in the boundary layer could cause surface warming, whereas heating near the UT/LS causes surface cooling and reduces precipitation[73].

ATMOSPHERIC EVOLUTION OF LACs

The evolution of LACs in the atmosphere since emission includes complex processes of LACs interacting with gases, water, and other pre-existing particles. The physical processes (e.g., condensation and coagulation) and/or chemical reactions (e.g., oxidation) are involved during the evolution, hence the properties of LACs are modified. For BC-containing particles specifically, aging is due to the accretion of non-BC materials and their chemical evolution, and changes in the particle morphology. The refractory material itself is not known to age.

Aging of BC

Freshly emitted BC particles, particularly from fossil fuel burning, are fractal aggregates and hydrophobic[19], with little additional non-BC materials coated on them. After emissions, BC particles go through further restructuring[19] by internally mixing with other aerosol components[74]. The restructuring and coating/mixing processes after emission are often known as BC aging. Observations have shown that BC typically ages within a few hours over polluted regions such as urban and biomass-burning areas[75,76] due to high rates of condensation and coagulation, whereas the aging timescale can be days to weeks in remote areas, as suggested by some observation-constrained modeling studies, e.g., refs. [77,78]. Globally, the condensation–coagulation processes dominate BC aging over the tropics and mid-latitudes, while heterogeneous oxidation processes are more important for BC aging over the two polar regions[78]. During aging, BC aggregates tend to collapse from lacy structures to being more compact with larger fractal dimensions (2.0–2.5) and particle sizes, varying with aging conditions[25].

The traditional Lorenz–Mie theory has been commonly used to compute the enhanced BC mass absorption efficiency when a spherical BC core is engulfed by a concentric spherical shell of non-BC substance[79]. Observations have indicated that BC coating during aging enhances its light absorption by up to a factor of 2 relative to uncoated BC[80–82], whereas some measurements[83] found rather weak (~6%) enhancement in BC absorption during aging. This can be explained by the strong dependency of BC optical properties on its coating structures such as coating thickness and composition, particle compactness and size, and specific coating shapes[84]. Light scattering from BC can be much more strongly affected by physical arrangement and association with non-BC materials, but this is usually very small in terms of the total aerosol scattering properties.

Recent observations[81] revealed that BC absorption enhancements during aging are correlated with the mass ratio of non-BC to BC components of the particle, with strong enhancements for larger ratios (e.g., >3 from biomass-burning emissions) and weak enhancements for small ratios (e.g., <1.5 from fresh traffic sources). Most BC particles are initially emitted into the transition regime (ratios of 1.5–3) according to global emission inventories. Theoretical studies have further pointed out that the interactions between the pure BC component and non-BC coatings are rather

complex (e.g., shadowing and necking effects), and assuming core-shell structures or homogeneous spheres with volume mixing for coated BC particles can cause significant biases in BC optical properties by up to more than a factor of 2, e.g., refs. [85–87]. Hence, better characterizations of BC particle structures during aging in both measurements and modeling studies are needed. An additional consequence of the aging processes is the increased hygroscopicity of BC-containing particles and their likelihood to serve as CCN. Aging can also change the BC-containing particle ice nuclei (IN) activity[88].

An appropriate representation of BC mixing state in individual particles is therefore important in studying its optical and hygroscopic properties. Riemer et al.[89] summarized the current approaches on modeling the mixing state of aerosol. Mixing state as treated in 2D size-resolved[90] or single-particle-resolved[91] schemes will improve the realism of treatments of BC associated with other substances. Particle-resolved model simulations have shown that the light absorption of BC could be erroneously overestimated by a factor of up to two if only considering the bulk-averaged composition[92], and such a process-level model has also been applied to investigate the CCN ability of multi-component particle[93].

Modeling on BC aging

BC atmospheric aging is one of the key uncertainty sources in modeling BC and its associated global burden and radiative effects[47,78]. Typically, global climate and chemical transport models assume a globally uniform e-folding aging time (1–2 days) to convert hydrophobic BC to hydrophilic BC[2,47]. This simplified e-folding scheme implicitly accounts for BC aging caused by condensation of soluble materials, coagulation with pre-existing particles, and other possible processes using a single tunable aging timescale.

However, a uniform e-folding timescale of 1–2 days significantly underestimates BC aging rates over polluted regions based on observations[75,76], and is likely one important contributor to the high biases in global BC simulations, particularly over remote regions[47]. The AeroCom model ensemble captured the vertical pattern of BC concentration in the southern mid-high latitudes but overestimated the concentration in the upper troposphere over the remote Pacific[94]. Model approaches to reduce these biases have largely focused on increasing BC aging rate[77] and/or removal of BC via wet deposition[95]. Further studies, e.g., ref. [77] attempted to optimize the e-folding aging time by constraining model results with observations, showing substantial variations in predicted aging rates for BC from different source regions.

To improve BC aging simulations, some global/regional models also adopt physically based aging parameterizations by quantitatively relating BC aging rate to key factors such as pre-existing gas and aerosol concentrations, atmospheric oxidant concentrations, emissions of coating precursors, and particle sizes to account for condensation and coagulation aging processes[90,91]. However, these parameterizations are limited by assumptions made during their developments. Further studies, e.g., ref. [78] have developed a hybrid microphysics-based BC aging scheme for application, which not only accounts for microphysical aging processes but also retains the computational efficiency of simplified aging parameterizations, which significantly improves global BC distributions in a chemical transport model (Fig. 5). Currently, the most accurate BC aging simulations are from models that have fully fledged dynamic aerosol microphysics and resolve particle sizes, e.g., refs. [91,96], although they require heavy computations. Another potential limiting factor is BC aging caused by heterogeneous oxidation, which is still not fully understood but has been studied, e.g., ref. [97].

Aging of BrC

BrC is not chemically stable like BC, and can volatize, bleach, or be generated from secondary processes, e.g., ref. [3]. Hence, BrC absorption contributions vary more than those of BC after initial emissions. BrC with lower MW can be photolyzed and degraded to be less absorbing when directly exposed to solar radiation (i.e., photobleaching), but with different photolysis rates for certain chromophores[98]. Zhao et al.[99] observed a decay-time of minutes to few hours for three types of nitrated aromatics in solution due to direct photolysis or OH exposure. Forrister et al.[100] found that BrC in biomass-burning plumes decayed with a half-life of 9–15 h. The higher-MW and less-volatile BrC, such as a portion of combustion-generated BrC, was observed to be more resistant to photobleaching[101]. Therefore, the photobleaching rate of BrC is source- and species-dependent. Recent laboratory studies[102] suggested that certain chromophores could be formed through

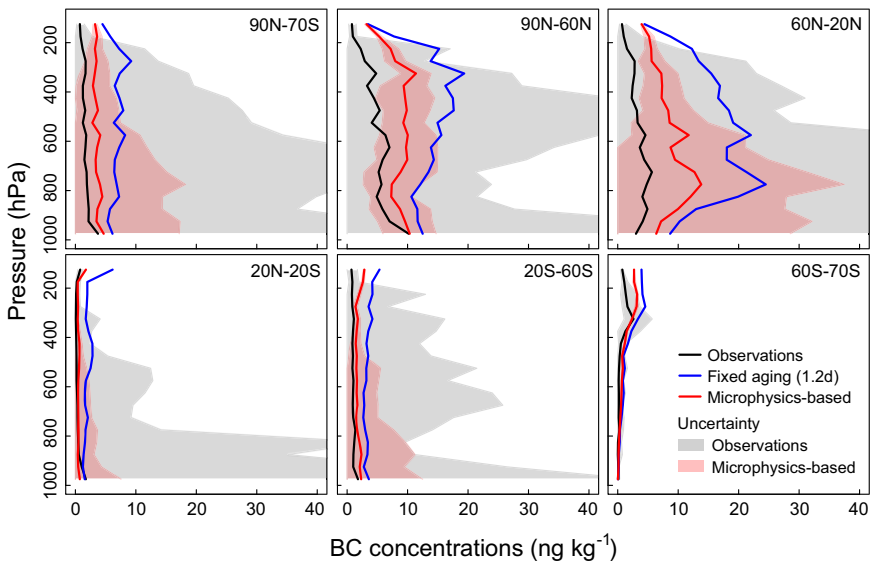

Fig. 5 Model-measurement comparison on the vertical distribution of BC. Comparisons between the HIAPER Pole-to-Pole Observations (HIPPO; black) and GEOS-Chem model simulations with a fixed BC aging scheme (blue), and a microphysics-based aging scheme (red). Median vertical profiles of observations and model results are averaged over different latitudinal bins. Shaded areas are observational variabilities and aging-related model uncertainties. (Reprinted with permission from ref. [78]. Copyright 2016 Copernicus Publications).

a range of photochemical reactions in the aqueous phase to form the secondary BrC, thereby photo-enhancing the particle brownness. Increased O:C ratio was found to be correlated with the increase of BrC light absorption[103]. It is therefore important to understand photo-enhancement and photobleaching at the molecular level, in order to accurately quantify the timescale, species-dependency, and impacts of these two compensating processes.

It has been long established that the nitrogen-containing organic compounds are brown[104]. Emerging observations show that NO_3 oxidation, in particular at nighttime or by ammonia uptake[105], enhances the brownness through heterogeneous oxidation in the particle phase, e.g., by forming nitrated HULIS[106], polycyclic aromatic hydrocarbons (PAHs)[107] or toluene-SOA under high NO_x[108]. The change in particle morphology of co-existing BC and BrC could also affect the absorption of BrC[109]. In addition, the outside viscous layer may inhibit the BrC-related molecular diffusion under low RH[110].

Modeling on BrC optics and aging

Only a few modeling studies have tried to include BrC and to estimate its climate impacts, which are summarized in Table 2. Most of the models used a similar bulk method to simulate BrC absorption based on an a priori MAC, and scaling its concentration to an empirically determined fraction of organic aerosol (OA) mass concentration[95,111]. Some models assign a fixed MAC for all OA from specific sources. In addition to primary BrC from biomass and biofuel sources, some models also treat aromatic SOA as BrC, but with one order of magnitude lower MAC than that from biomass burning. No model has included fossil fuel sourced OA as BrC, although observations showed that they could contain BrC, e.g., ref. [112]. A more detailed approach is to parameterize the assumed imaginary refractive index of BrC to an independent variable such as MCE[113] or BC/OA ratio[20,114,115] to allow BrC properties to be tied to burning conditions.

As BrC absorption may change during chemical aging, models must deal with this additional complexity. A recent study by Wang et al.[114] includes a bleaching scheme assuming that the absorption of BrC decreases at a rate related to OH oxidation, with a specified minimum absorption. This parameterization is chosen to represent the observed BrC absorption lifetime of ~1 day[100,116], also used by studies[115,117]. As shown in Fig. 6, Wang et al.[114] estimated that the global mean DRF of BrC decreases from +0.102 to +0.048 $W\,m^{-2}$ after including the bleaching scheme. Some models also considered the effect of BrC internally mixed with BC, further enhancing the total absorption of BC-containing particles to some extent by the absorbing shell of coated BC, e.g., ref. [118].

Challenges remain in evaluating the modeled BrC global distributions and properties due to the lack of observations. Most modeling studies evaluate model skills by using AAOD from satellite or ground-based remote measurements, which however are unable to accurately discriminate BrC absorption from that of other aerosols (primarily BC)[116,119]. Some studies[114,115] have compared model simulations to in situ measurements obtained by solvent extraction (in water and organic solvent) of aerosol filters collected during aircraft campaigns over North America. Although the solvent extraction method can directly constrain BrC absorption, it still has limitations on evaluating model assumptions. The uncertainty results from the incomplete extraction of BrC in the air and transferring the bulk measurement to the airborne absorption. The latter is corrected using a conventional factor of 2 obtained at aerodynamic diameter of 0.5 μm[120], but this needs to be applied with caution due to the uncertain size-resolved absorption and the variability of sources[121].

ATMOSPHERIC REMOVAL OF LACs

Aerosols can be removed from the atmosphere by either deposition onto a surface or via chemical transformation. Deposition can occur with (wet) or without (dry) interactions with cloud/precipitation. LACs are subject to the same depositional removal mechanisms as total aerosols, with specific dependences relevant to the type of LACs. For BC, atmospheric removal largely depends on the particle hygroscopicity and size that are altered by ageing processes, while for BrC, species-specific chemical removal as discussed above is also important. Wet removal occurs either via cloud particle formation and subsequent conversion to precipitation (in-cloud removal or rainout) or impaction processes with hydrometeors below clouds during precipitation (below-cloud removal or washout), as the right panel of Fig. 2 illustrates. Aerosols can stay in clouds (without deposition) if the precipitation does not occur, and aerosols in cloud water could also be released back to the interstitial phase when the cloud particle evaporates, thus leading to several cycles for the cloud processing of aerosols. Finally, aerosols can exist interstitially in clouds (i.e., without association with cloud droplets).

In-cloud scavenging

In-cloud processing of aerosol includes the activation of aerosol particles to form liquid droplets or ice particles, collisions between hydrometeors and aerosols, and hydrometeor evaporation to release aerosols. Nucleation scavenging is one of the most important routes for aerosols to be incorporated into cloud particles. In this case, activated particles serve as cloud condensation nuclei (CCN) or ice nuclei (IN). This section discusses the CCN and IN abilities of BC, while BrC behaves as organic aerosols for this mechanism but cloud processing may modify its brownness. Aerosol particles need to be larger than a certain size (to provide sufficient surface) to be activated as CCN (generally > ~100 nm)[122]. Smaller particles (<20 nm) and larger particles (>a few microns) are preferentially removed by Brownian diffusion and gravitational settling, respectively[123]. Because LACs are mostly populated at the accumulation size mode from a few tens to hundreds-nanometers, the nucleation scavenging is its main removal process in the atmosphere[124].

Activation in liquid water

Köhler theory indicates that the water gas-particle equilibrium can be expressed by combined effects over a flat surface following the Raoult (solute) term and a curved particle surface in Kelvin (surface tension) term. Hence, water vapor has to reach a critical supersaturation (SSc) to activate the particle to be a stable droplet. Before reaching SSc, the dry aerosol must deliquesce (incorporate liquid water) and experience hygroscopic growth. Pure BC is water insoluble and must be internally mixed with water-soluble substances to allow hygroscopic growth and activation as CCN.

Previous laboratory studies[80,125] found that sulfate coatings promoted hygroscopic growth of soot, and organic coatings had limited contribution to overall hygroscopicity. Ambient characterization of the hygroscopic growth of BC was achieved with SP2 measurements, either via coupling with a conventional growth factor (gf) measurement for BC specificity[126,127] or using modified humidified SP2 to monitor the change of scattering properties after hygroscopic growth[128,129]. Both less (gf ~ 1.05) and more (gf ~1.4–1.6) hygroscopic modes of BC were found in the ambient[127], with the latter associated with BC coated with more water-soluble substance. It was also found that the volume mixing rule by applying the prescribed gf of known aerosol composition can predict the gf of BCc within 30%[127]. The main limitation of this system is its ability to investigate only certain particle sizes, while the composition and/or hygroscopicity of BCc is size-dependent. A

Table 2. Summary of models on BrC.

Reference	Model	Global/ regional	BrC sources	Optical properties for MAC calculating	Whitening	Mixing with BC	Evaluating with observations	BrC absorption DRE at TOA	Footnote
Park et al., 2010[220]	GEOS-Chem v7.04	Regional (East Asia)	Based on BrC/BC ratio	Based on Alexander et al. (2008)[221]	No	Externally mixed	Evaluate overall BC+BrC absorptions with surface measurements	0.05 W m^{-2}	a
Feng et al.[148]	IMPACT	Global	2/3 of biomass and biofuel POA	Moderately absorbing case: based on ref. [21], Strongly absorbing case: based on Kirchstetter et al. (2004)[222]	No	Internally core-shell	Evaluate overall BC+BrC absorptions with AERONET AAOD	Moderate absorbing case: 0.04 W m^{-2} Strongly absorbing case: 0.11 W m^{-2}	b,c
Lin et al., 2014[223]	IMPACT	Global	Biomass and biofuel POA; Biomass-burning SOA	Moderately absorbing case: based on ref. [21], Strongly absorbing case: based on Kirchstetter et al. (2004)[222]	No	Externally mixed	Evaluate overall BC+BrC absorptions with AERONET AAOD	Moderate absorbing case: 0.22 W m^{-2} Strongly absorbing case: 0.57 W m^{-2}	c
Jacobson, 2014[224]	GATOR-GCMOM	Global	Assume 30% of biomass and biofuel POA as strongly absorbing BrC; Assume other 70% as moderately absorbing BrC	Moderately absorbing case: based on Alexander et al. (2008)[221]; Strongly absorbing case: based on Kirchstetter et al. (2004)[222]	No	Internally core-shell	Evaluate total aeroso absorptions with AERONET and OMI AAOD	Not reported	b
Wang et al.[123]	GEOS-Chem v9.1.3	Global	50% of biofuel POA; 25% of biomass POA; Aromatic SOA	Br-POA: based on ref. [21] (Liu et al. 2013[120]; Zhang et al. 2013)[225]; Br-SOA: based on Zhang et al. (2013)[225]	No	Externally mixed	Evaluate overall BC+BrC absorptions with AERONET AAOD	0.07 W m^{-2}	c,d
Saleh et al.[26]	GEOS-Chem v9.1.3	Global	Biomass and biofuel POA	Based on the simulated mass concentration ratio of BC/OA and parameterization of ref. [20]	No	Externally mixed	No evaluation.	0.12 W m^{-2}	c,e
Wang et al., 2016[226]	GEOS-Chem v9.1	Regional (Amazon)	Biomass and biofuel POA	Based on the emitted ratio of BC/OA and parameterization of ref. [20]	No	Externally mixed	Evaluate overall BC+BrC absorptions with AAOD	Not reported	
Wang et al.[152]	GEOS-Chem v10.1	Global	Biomass and biofuel POA; Biomass SOA	Based on the emitted ratio of BC/OA and parameterization of ref. [20]	Yes	Externally mixed	Evaluate with direct BrC absorption from aircraft measurements	0.048 W m^{-2}	c,d
Brown et al.[153]	CESM with CAM5.4	Global	Biomass and biofuel POA	Based on the emitted ratio of BC/OA and parameterization of ref. [20]	Yes	Internally mixed (volume mixing)	Evaluate overall BC+BrC absorptions with AAOD	0.06 W m^{-2}	c
Zhang et al.[126]	CESM with CAM5	Global	Biomass and biofuel POA; Aromatic SOA	Br-POA: based on the emitted ratio of BC/OA and parameterization of ref. [20] Br-SOA: based on Nakayama et al. (2010)[227]	Yes	Externally mixed	Evaluate with direct BrC absorption from aircraft measurements	0.1 W m^{-2}	c,f

[a]Absorption DRE is the Asian mean of annual average values.
[b]Both non-absorbing OA and BrC are assumed to be coated on BC and cause lensing effect. The effect from reduced externally mixed BrC due to coating is not considered.
[c]Absorption DRE is the global mean of annual average value.
[d]BrC are assumed to be externally mixed with BC. Non-absorbing OA are assumed to be coated on BC and cause lensing effect.
[e]Both non-absorbing OA and BrC are assumed to be coated on BC and cause lensing effect. The effect from reduced externally mixed BrC due to coating is also considered.
[f]A convective transport of BrC was included: the wet scavenging efficiency of BrC was decreased to force more BrC transported through convection to the free troposphere.

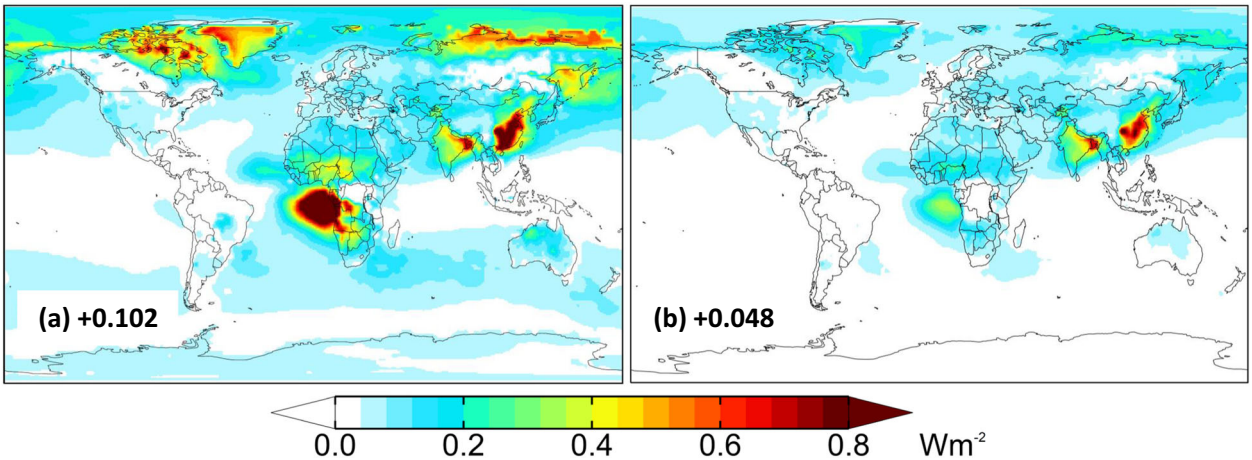

Fig. 6 Modelled BrC radiative effects. Brc Global annual mean direct radiative forcing resulting from the BrC absorption at the top of the atmosphere (TOA) in 2014, before (**a**) and after (**b**) incorporating the modified BrC bleaching scheme. (Reprinted with permission from ref. [114]. Copyright 2018 Copernicus Publications).

recent study, using detailed compositional information for BCc, is able to derive the size-dependent hygroscopicity of BCc, and found a consistent minimum hygroscopicity at particle diameter of 100 nm[130]. Direct measurements of the CCN activity of BCc under supersaturation is sparse. A previous study found that a coating thickness of 10 nm on the less-volatile aerosols leads to CCN activation for half of the aerosol population at SS = 0.5%[131]. By using Single particle measurements[132], Ding et al.[132] found that a low SS = 0.08% can activate ~50% of the BC particles in a highly polluted environment over East Asia, when the BCc can grow to a very large size with a count median diameter of ~0.28μm.

Though it is not a widely approached manner for previous studies in isolating the absorbing component (BrC) from all organic aerosols, the discussion here gives a general summary of the key factors influencing the water processing on BrC. The CCN ability of organic aerosols was conventionally believed to be lower than inorganic salt, due to their lower water solubility. Previous studies found that freshly emitted biomass-burning aerosols show weak hygroscopic growth under sub-saturated conditions[133] and low CCN activity at artificially created supersaturated conditions[134]. A number of studies represented the oxidation state of organics using the O/C atomic ratio obtained from the AMS[135], and linked this parameter with hygroscopicity, showing either enhanced growth with increased O/C[136] or not well correlated[137].

The aqueous processing of BrC in aerosol water or clouds may modify its brownness. The water medium could facilitate the oligomerization or polymerization reactions to enhance the absorption by connecting multiple chromophores, such as the identified formation pathways of HULIS[5,138]. BrC absorption could be dynamically modified in cloud microdroplets, where the loss or addition of water through evaporation or condensation (as the PH value changes) potentially leads to hydrolysis or dehydration[139]. The dehydration could lead to a higher fraction of unsaturated compounds from alcohol to enhance the brownness, while the hydrolysis decreased the absorptivity[140].

A solution containing materials with different solubility may have complex morphologies if the less-soluble substances present as shells fully or partly engulfing the soluble core[141]. Although it is still not clear how BrC is redistributed in the particle, the amphiphilic organic surfactants present at the air-solution interface can largely promote the CCN activity by reducing the surface tension[142,143]. For surface-active shells (such as the candidate HULIS) that are light absorbing, associated light absorption in clouds has not been fully explored.

Activation in ice

Above about −38 °C, a water droplet requires an IN to freeze via heterogenous ice nucleation. When the droplet exists before ice nucleation, the IN can interact with the droplet by immersion within it or contact (touching the droplet). Alternatively, the IN can nucleate ice directly from water vapor through the deposition mode.

Many studies suggested that combustion particles are inefficient IN, regardless of the mode of ice nucleation[144] and references therein, which however is still under debate. A certain type of soot made by a spark generator may show efficient deposition IN below 240 K[145], but its atmospheric relevance is not clear. Measurements of IN with and without removal of rBC showed that rBC accounts for about 40% of all IN numbers for some biomass emissions[146]. BC may act as a contact IN at temperatures between 245 and 251 K[147]. Mixing with other water soluble or colloidal substance could modify the surface properties of BC and hereby IN activity. Flaming soot produced with different organic contents showed that the organic coatings decreased the IN efficiency in the deposition mode compared to the bare counterpart[148]. Observations[149] using different soot types in the cloud chamber revealed that BC with a higher OC content (>20%) showed lower deposition IN than that with an OC content of <20%.

A consistent finding among many studies is the moderate activity of BC as immersion IN at high ice activation temperatures, i.e., generally above −30 °C[147,150,151], but small activity as deposition IN at the homogenous IN temperature (<−38 °C, but below the homogenous freezing threshold of the solution). A recent study[152] investigated the IN activity of soot particles with a range of particle morphologies and mixing states at −40 to −50 °C, and confirmed the deposition IN capabilities of bare BC and the degradation of this ability due to coatings. Hence coated BC requires a higher ice supersaturation to act as IN near the homogenous freezing threshold.

The IN properties of OA have been reviewed by Knopf et al.[153]. Unlike the solid BC particle, the phase of OA, as determined with viscosity measurements, changes according to ambient temperature and RH. Increased temperature and/or RH will transform OA from a glassy-solid to the liquid phase when above the deliquesce RH, and enters a transitional phase state under partial deliquesce RH when the phase appears as semi-solid with moderate water content[154]. In the glassy phase, highly viscous OA may serve as deposition IN, and OC at semi-solid may provide some active sites as immersion IN. These issues are also relevant to SOA specifically[155]. HULIS, depending on its viscosity state, can act as

immersion IN in supercooled droplets or as deposition IN under lower supersaturation, as shown in ambient measurements[156]. Given that a considerable fraction of HULIS is light-absorbing, these BrC species incorporated in ice crystals may potentially perturb cloud microphysics.

Both laboratory and field studies tend to agree that the solid and insoluble surface can provide ice-active surfaces for deposition mode IN, while any added/transformed/formed soluble substance on the insoluble/less-soluble substance tends to transform the particle into an immersion mode IN. This transformation is essentially determined by the ambient temperature, vapor pressure and the amount of each specified species in a particle. It is therefore important to tackle the evolution of BC and BrC properties during the ageing process to understand their IN activities.

Aviation provides an anthropogenic source of pollutants that are directly emitted into the UT/LS. This can add additional IN in the region and may perturb the microphysics of cirrus. Introducing aviation emissions may decrease (increase) the ice numbers hereby leading to optically thin (thick) cloud optical depth and decrease (increase) its longwave radiative warming[157]. The presence of heterogenous IN in the homogenous regime may suppress the freezing from the liquid solution by competing the water vapor. Kärcher et al.[144] found that an initial addition of heterogenous IN to the existing solution particles can reduce the ice number, but further increase of heterogenous IN will increase the ice number. Such sensitivity depends on the updraft and the availability of moisture. The contribution of BC from aviation emissions to the modification of high-level cirrus cloud microphysics remains uncertain, partly due to the inconsistently assumed BC ice nucleation ability and supersaturation threshold of ice nucleation in models[124,158]. A 20-year projection analysis[159] showed that absorbing emissions from aviation may perturb atmospheric stability at the cruising altitudes by suppressing cumulus clouds at lower altitude, and enhancing stratiform cloudiness.

In situ measurements of nucleation scavenging

In addition to laboratory characterizations of aerosol activation under prescribed conditions, residues from cloud droplets have been measured from ambient clouds for decades, by sampling on the ground encountering orographic clouds, e.g., refs. [160,161], fogs, e.g.,[162,163], or clouds via aircraft, e.g.,[164,165]. Many approaches use a heated inlet to sample all (in-cloud and interstitial) particles and a conventional inlet with an aerodynamic cut-off above ~1 micron in diameter (thus not containing cloud particles) to sample interstitial particles. The difference between the two sampling lines was deemed to represent aerosol residues to cloud droplets. This technique has been long used at an alpine site to investigate the liquid and mixed-phase orographic clouds[160,166]. Another powerful approach is to directly characterize the residues by separating cloud drops from interstitial aerosols with a counterflow virtual impactor (CVI)[167], which uses a barrier flow of filtered air to reject particles below a certain size (usually a few microns). Then dry, warm air is used to evaporate the water component of the droplets to release the residuals for subsequent detection. This technique has been applied in aircraft[164,165] and on the ground[168]. The nucleation scavenging efficiency of BC showed large variabilities in these studies, which is either moderate[166] or negligible[164].

Liquid water–ice interaction

Particle removal efficiency in mixed-phase clouds is particularly important, as it is associated with the temperature regime in which most precipitation is formed. The co-existence of supercooled liquid water with ice particles alters the nucleation activation processes that occur in warm clouds, mainly based on two main mechanisms. One is the Wegener–Bergeron–Findeisen (WBF) process where water vapor is supersaturated over ice but sub-saturated over water. The ice crystal will grow in expense of liquid water, while the CCN included in supercooled water droplets will be released back to the interstitial phase. The other one is the riming process where liquid droplets are directly accreted to large ice particles without being evaporated. The WBF or riming process exerts contrasting effects, lessening or enhancing aerosol scavenging, respectively. Previous studies often used BC as an unreactive tracer to evaluate these cloud-relevant microphysics processes. These processes are sensitive to the assumed BC mixing state, e.g., an increased externally mixed hydrophobic BC concentration may enhance the ice nucleation and promote the riming process and cloud loss[169]. Long-term measurements[166] at an alpine site influenced by orographic clouds showed that the scavenging efficiency of BC was reduced from 60 to 5–10% when the ice mass fraction of clouds increased from 0 to >0.2. Measurements[170] at an Arctic site with predominantly rimed snow particles revealed that BC scavenging efficiency tended to increase by 10%. A recent study[161] documented a precipitation event that successively experienced the riming process by graupel and then the WBF process by snow precipitation, with contrasting shifts of BC core sizes in the interstitial phase associated with the two processes. Riming led to preferential removal of particles with larger BC cores, while the WBF process released some of the BC cores that had been incorporated in liquid droplets. Inclusion of WBF processes in models has been shown to improve simulations of BC concentration[171,172].

Light absorption by LACs in clouds

The heating effects of LACs when incorporated within a hydrometeor is only considered in limited studies, e.g., refs. [124,173]. The approach assumes that the absorbing aerosol inclusion is randomly dispersed throughout a hydrometeor particle, with the overall effective refractive indices determined by an interactive dynamic effective medium approximation (DEMA)[174]. Globally, they showed that BC inside hydrometeors and in the interstitial phase could lead to additional heating rates of 200% and 130%, respectively, compared to BC under clear sky. Liou et al.[175] pointed out that accounting for BC absorption in cirrus clouds substantially increases total absorption causing important warming impacts.

BELOW-CLOUD SCAVENGING

Below-cloud scavenging of aerosols occurs during falling precipitation. The raindrop collection efficiency of particles depends on the raindrop and particle size spectra, and the drops' terminal velocity. Smaller particles are subject to removal due to Brownian diffusion, and larger particles are removed via impaction/interception because larger inertial mass is less likely to move out of a drop's path. Cloud models indicate that although nucleation scavenging dominates the overall removal of water-soluble aerosols, impaction scavenging still provides an important removal mechanism for hydrophobic aerosols, in particular for BC that is not internally mixed with other hydrophilic materials[176]. Wang et al.[177] pointed out large model underestimates of below-cloud scavenging of aerosols by 2–3 orders of magnitudes compared to field measurements, which may result from the treatments of cloud microphysics and dynamics. Ohata et al.[178] performed ground-based measurements of BC size distribution in air and in rainwater to constrain total wet removal of BC during precipitation events, and estimated that impaction scavenging of BC was responsible for one tenth of total removal.

Characterization of overall wet deposition

The total (in-cloud and below-cloud) wet removal of aerosols has been long studied by collecting precipitation water and measuring the concentration of particulate species in it, as reviewed by Herckes et al.[179]. However, such measurements typically are unable to separate rainout and washout contributions[180] or to identify the location where the scavenging was initiated. Offline analysis on the composition in rainwater was performed to characterize OC/EC concentration[181], rBC[182], and to isolate the water soluble and insoluble OC[162]. A few studies also investigated the brownness of cloud water or rainwater[183,184]. By comparing BC concentrations in the water and in the ambient air, some studies obtained the wet scavenging efficiency of BC, showing a general consensus that freshly emitted BC has a lower scavenging efficiency than aged BC at remote sites[180] and references therein.

Another widely used approach to constrain aerosol removal is to estimate the scavenging efficiency by comparing the measured concentration with a chemically and hygroscopically inert species, such as CO. Over the timescale of weeks, BC is subject to removal along the transport pathway, yet CO is not. Hence, a decrease of the net concentration (i.e., concentration difference relative to background) ratio ΔBC/ΔCO occurs when BC is at least partly scavenged. This method, however, requires an assumption of the concentration ratio at emission. Liu et al.[185] used footprint source attributions with emission inventories to estimate ΔBC/ΔCO from sources and further estimated the BC scavenging over the Arctic. A few studies[186,187] measured ΔBC/ΔCO at a receptor site between air masses with and without precipitation after emissions to obtain the BC scavenging linked with the accumulated precipitation along the transport pathway. They showed an exponential decay of BC concentration correlating with the amount of precipitation[186,187], which however was not observed in the free troposphere of the Arctic[185].

Modeling on LAC wet deposition

Typically, global models use first-order wet scavenging treatments for BC, OC and other aerosols. Current model treatments of BrC wet deposition generally follow those of OC. For BC or OC in-cloud scavenging, it is generally treated as follows, e.g.,[188]:

$$F_i = f(1 - e^{-k_i \Delta t}),\ k_i = k(R_i f_{i,L} + f_{i,I}), \quad (3)$$

where F_i is the fraction of aerosols scavenged in clouds during a time step (Δt), f is the horizontal areal fraction of the grid experiencing stratiform and convective precipitation, k_i is the first-order in-cloud loss rate, $f_{i,L}$ is the fraction of aerosols present in the liquid (ice) condensate, k is the conversion rate from cloud (ice and liquid) condensate to precipitation, and R_i is the retention efficiency of aerosols in liquid clouds. The below-cloud scavenging follows the similar parameterization as in-cloud removal but with a different formulation for the first-order loss rate (k_i) based on the first-order washout rate constant (determined by aerosol-droplet collision-collection processes) and precipitation rate. Re-evaporation of precipitating droplets and the induced re-release of aerosols are typically considered in models too. For scavenging in convective updrafts, it follows a similar treatment:

$$F_i = f(1 - e^{-k_i \frac{\Delta z}{w}}), \quad (4)$$

where w is the updraft velocity and Δz is the lifted distance.

Later studies[189,190] improved the aerosol scavenging rate constants by accounting for effects of aerosol size, different below-cloud removal efficiencies in rain/snow events, BC removal from heterogenous and homogeneous ice nucleation processes, and updated BC scavenging efficiency in convective updrafts. Direct modifications of removal in convection and scavenging efficiency have been demonstrated to improve BC predictions at high altitudes[95,191]. Recent studies, e.g., ref. [192] further included the WBF process of BC in models based on parameterizations derived from observations, which improves simulated global BC distributions and wet deposition fluxes. Some studies, e.g., refs. [193,194] also applied physically based parameterizations of BC ice nucleation to investigate its effects on ice cloud processes, which however has not been fully coupled with the BC wet scavenging process. More accurate microphysical treatments of BC aging and/or wet deposition (typically reduced scavenging of BC in ice or mixed-phase cloud) improved model representations of the BC distribution in the Arctic[189,192], though still showing difficulties in capturing the BC seasonal variation on the ground, particularly in spring and winter[171,189,195]. Modeling studies specifically on assessing and enhancing BrC wet deposition simulations are yet unavailable.

Dry deposition

Dry deposition refers to the direct removal of particles from the atmosphere to Earth surfaces by gravitational settling, impaction, interception, and diffusion, without interaction with water hydrometeors. Atmospheric turbulence parameters in the surface boundary layer, e.g., the friction velocity, are key components in dry deposition parameterizations. Dry deposition of BC is differentiated from total aerosols because of its unusual morphologies and size (see Sections on emission and ageing), which influence its impaction losses. Emerson et al.[196] conducted direct measurements of dry deposition fluxes of BC mass and number over a grassland using the eddy covariance flux technique, and obtained a positive mean rBC dry deposition of 0.3 ± 0.2 mm s^{-1}. This result however cannot be generalized to represent the full range of deposition rates for different morphologies of BC or over different types of surfaces. The BrC and tar balls may be more associated with spherical particles of intermediate density, following that of total aerosols. Present models typically follow an empirical resistance-in-series framework[197] to simulate aerosol dry deposition depending on meteorological conditions and local surface type, which however shows large uncertainties. In the past decade, a number of studies, e.g., refs. [198,199] have attempted to improve the parameterization of dry deposition velocity within this framework, leading to better model simulations of BC concentrations such as in the Arctic[200]. Moreover, the dependence of dry deposition velocity on particle morphology has not been accounted for in present models, which may be important particularly for BC-containing particles with complex structures.

Deposition of LACs in the cryosphere

When LACs are deposited onto snow/ice surfaces in the cryosphere, they can significantly reduce the surface albedo[201–203]. This triggers a strong surface radiative forcing and eventually a positive snow albedo feedback[204]. This further results in enhanced regional warming over the northern high-latitudes and mid-latitude mountains[205,206]. A number of field measurements have been conducted to measure BC concentrations in snow over the global cryosphere[204] and reference therein. Overall, BC concentrations in surface snow show strong spatiotemporal heterogeneity across the globe, with mean values of roughly 500, 30, and 20 ppb in Northern China, North America, and the Arctic, respectively, which produce snow albedo reductions of 0.02–0.09, 0.004–0.015, and 0.003–0.011 depending on snow grain size and BC-snow mixing type[207,208]. Within each of these regions, the sub-regional variation of BC concentration in snow is also substantial, up to 1–2 orders of magnitude[208]. Further, it is possible that the size distribution of BC in snow can be significantly different from that in the air, and exhibit a different MAC[209], which could lead to nontrivial impacts on snow albedo[210]. Thus, accurate estimates of BC-snow albedo effects require more extensive concurrent measurements of BC distributions in snow and surface albedo/reflectance over the global cryosphere, particularly in regions with strong spatiotemporal heterogeneity.

Direct measurements of BrC in snow are limited in the global cryosphere, due to the complex nature of BrC, which is only raised in the communities' consciousness within the past 10 years. Several field campaigns attempted to measure soluble BrC concentrations in snow over Asia[211,212], North America[213], and the Arctic[213]. Some of these measurements, e.g., ref. [213] used optical methods (e.g., spectrophotometer) to analyze aerosol light absorption, which however is difficult to accurately separate BC, BrC, and dust. Other studies, e.g., ref. [211] also measured water-soluble BrC in snow and its optical properties, but it should be noted that the BrC dissolved in snow medium cannot be treated in the same way as solid particles like BC/dust in snow radiative transfer models to compute BrC-induced albedo reduction. Thermal measurements[212] have been applied to separate BC and OC in snow-loaded filters, but this approach is unable to differentiate BrC from non-absorbing OC. Dang and Hegg[214] proposed to combine optical methods with serial chemical extractions to analyze the light absorption of different non-BC components (i.e., BrC and dust). This might be a relatively accurate way to measure BrC absorption but requires reliable BrC optical properties to convert it to BrC content in snow. Recently, Beres et al.[215] measured spectral snow albedo reductions due to artificial BrC deposition, and found an instantaneous radiative forcing of about 2.7 W m^{-2} per ppm of BrC in snow. In addition to darkening the snow surface, BrC's optical impacts in the UV and short-visible wavelengths can alter photochemistry at the snow surface, such as nitrate/nitrite photolysis[216] and mercury and bromine chemistry[217]. Thus, more extensive and accurate measurements of BrC content and absorption in snow are needed to accurately quantify BrC effects on snow albedo and related photochemistry.

BC and BrC concentrations in snow are driven by their atmospheric deposition fluxes and post-deposition evolution in the snowpack. However, measurements of their deposition fluxes in the cryosphere and evolution in snowpack are very scarce. Recently, Yan et al.[218] for the first time provided direct in situ measurements of wet and dry deposition rates for BC and water-insoluble OC (WIOC) at three remote sites in the Tibetan Plateau, with large spatiotemporal variations and annual wet deposition rates of about 3–35 and 50–330 mg m^{-2} yr^{-1} for BC and WIOC, respectively. Some studies attempted to indirectly derive BC deposition rates from BC content in snow or ice cores based on certain assumptions, but with large uncertainties[85]. Direct measurements of how BC/BrC evolves during different snowpack processes after deposition, for example by meltwater scavenging, are also rare[202,204]. More field and laboratory measurements of BC and BrC deposition and evolution in snowpack are needed to constrain their distributions in snow and subsequent radiative effects.

FUTURE DIRECTIONS

This review summarizes recent advances and up-to-date knowledge for the key atmospheric processes affecting LACs and their associated uncertainties. Processes discussed include emission, transport, evolution/transformation, and deposition. The relative importance of these processes on affecting LAC lifetime and climate impacts depends on many factors such as ambient conditions. The computational costs of increasingly sophisticated modeling efforts must be balanced against incorporation of more detailed process representations; hence models with different spatiotemporal scales and resolutions may benefit from different choices of the amount of details to include. Besides reducing the large uncertainty in emissions as emphasized in Bond et al.[2], we highlight the significant challenges that lie ahead and potential future directions in order to further reduce uncertainties in the estimates of LACs' abundancies and radiative effects.

Characterization of LAC properties by source

Remarkable differences in intrinsic properties have been shown for the LACs emitted from different sources, in particular between biomass/solid fuel burning and traffic-related sources. Such observables as OC/BC ratio, size distribution, degree of internal mixing, hygroscopicity, and optical properties vary with burning conditions, fuel type, and environmental conditions at emission. Models and inventories have incorporated some of the observed dependencies, but the community needs improved inventories and models to account for emission properties, such as in segregating the properties according to OC/BC ratio, burning phase or fuel types.

Size-resolved information

Size-resolved information is not widely available from both source and ambient measurements. Most models rely on bulk-only information, and assume a nominal size distribution. Process-level models may include size-resolved mixing state information for BC, but are not supported by current emission inventories or the advanced measurements necessary for model evaluation. Progress can be made with additional measurements of size-resolved composition of BC, OM, BrC (or bulk refractive index) at each size-bin, and such information should be obtained from both near-source and regional environment.

Time scales and variation of optical properties during LAC ageing

The rate coefficient of LAC aging and its impact on optical properties must be more clearly constrained to identify the best manner of parameterization. Presently, aerosol microphysics schemes using multi-phase and heterogenous chemistry based on thermodynamically consistent approaches are just starting to be included in modeling BC mixing and the subsequent solubility transformation. The decay rate of BrC is just starting to be modeled via reactions with oxidants. These advanced approaches, however, require stronger observational constraints. For example, although measurements of BrC evolution are still challenging, they may be required to map the absorptivity of organics to their volatilities and viscosities, an approach that has shown value for characterizing total organic aerosols.

Interactions with clouds

There is lack of direct field measurements to clarify the importance of particle size and composition in determining the CCN/IN-activity of BC-containing particles, and to inform the parameterization of BC ageing and its wet scavenging efficiency. BrC may act as a surfactant and promote CCN activation. It is essential to identify the stage (in terms of solubility or viscosity) during their lifecycle that LACs could efficiently interact with water vapor or existing water/ice hydrometeor. Improved understanding of ice and droplet nucleation on the phase of aerosols will help address large uncertainties in LAC removal and optical impacts in liquid water and ice. These important interactions with water and ice, combined with the timescale of ageing, determine the abundance of LACs in and out of clouds.

LAC light absorption in hydrometeors

The absorption of LAC in clouds can be enhanced compared to that in clear air. This has been believed to heat and evaporate clouds, but only a few advanced models consider this process. LACs' radiative impacts in clouds, both interstitially and within cloud hydrometeors, are highly uncertain. This should be better understood once the nucleation activity of LACs is more strongly constrained. The abundance of BC in snow has been studied since the 1980s, though its depositional flux on the snow surface remains to be directly measured. The BrC contribution to the

modification of snow albedo is only starting to be explored, but a reliable measurement to accurately quantify this is still challenging. Investigations of the post-deposition evolution of LACs within the snowpack are rare. In particular, improved understanding of modifications of the size distribution of LACs during snowpack processes and the scavenging efficiency by meltwater will be key in untangling LAC's impacts on snow albedo.

Coupled modeling-measurement opportunities

Inconsistencies between modeled and measured parameters of LACs need to be resolved. A specific problem is the conversion from measured absorption to the pre-defined composition of LACs in models. Commonly, a range of measurement techniques, each with its own intrinsic uncertainties, has been used to speciate LACs. Hence, ambiguity in speciation, either by measurements or models, results in biases in attributing the impacts of each type of LACs. At this point, with large uncertainties in the range of BrC optical properties in the ambient coupled with uncertainty in the chemicals directly driving those properties, a consistent and flexible theoretical approach to categorize different LACs' contributions to absorption is still needed. To aid the development of such a framework, a global data set containing consistent and explicit measurements available for consistent model evaluation would be very useful. This type of database is becoming more widespread for BC[191,219], but is likely a more challenging goal for BrC because of the remaining inconsistent measurement protocols.

Therefore, the lifecycle of LACs and associated detailed interactions with other atmospheric compositions, radiation, cloud, precipitation, and snow/ice are at the heart of their overall climate forcing uncertainty. Combined considerations for these aspects will enhance evaluating the radiative (both direct and indirect) and climate impacts of LACs in the Earth system.

DATA AVAILABILITY

All data related to this paper may be requested from the original publishers.

Received: 17 March 2020; Accepted: 5 September 2020;
Published online: 21 October 2020

REFERENCES

1. Bond, T. C. & Bergstrom, R. W. Light absorption by carbonaceous particles: an investigative review. *Aerosol Sci. Technol.* **40**, 27–67 (2006).
2. Bond, T. C. et al. Bounding the role of black carbon in the climate system: a scientific assessment. *J. Geophys. Res. Atmos.* **118**, 5380–5552 (2013).
3. Laskin, A., Laskin, J. & Nizkorodov, S. A. Chemistry of atmospheric brown carbon. *Chem. Rev.* **115**, 4335–4382 (2015).
4. Bergstrom, R. W., Russell, P. B. & Hignett, P. Wavelength dependence of the absorption of black carbon particles: predictions and results from the TARFOX experiment and implications for the aerosol single scattering albedo. *J. Atmos. Sci.* **59**, 567–577 (2002).
5. Andreae, M. O. & Gelencsér, A. Black carbon or brown carbon? The nature of light-absorbing carbonaceous aerosols. *Atmos. Chem. Phys.* **6**, 3131–3148 (2006).
6. Schulz, M. et al. Radiative forcing by aerosols as derived from the AeroCom present-day and pre-industrial simulations. *Atmos. Chem. Phys.* **6**, 5225–5246 (2006).
7. Reid, J., Koppmann, R., Eck, T. & Eleuterio, D. A review of biomass burning emissions part II: intensive physical properties of biomass burning particles. *Atmos. Chem. Phys.* **5**, 799–825 (2005).
8. McMeeking, G. R. et al. Emissions of trace gases and aerosols during the open combustion of biomass in the laboratory. *J. Geophys. Res. Atmos.* **114**, D19210 (2009).
9. Ting, Y. et al. The mixing state of carbonaceous aerosols of primary emissions from 'Improved' African cookstoves. *Environ. Sci. Technol.* https://doi.org/10.1021/acs.est.8b00456 (2018).
10. Claeys, M. et al. Chemical characterisation of humic-like substances from urban, rural and tropical biomass burning environments using liquid chromatography with UV/vis photodiode array detection and electrospray ionisation mass spectrometry. *Environ. Chem.* **9**, 273–284 (2012).
11. Lin, P., Rincon, A. G., Kalberer, M. & Yu, J. Z. Elemental composition of HULIS in the Pearl River Delta Region, China: results inferred from positive and negative electrospray high resolution mass spectrometric data. *Environ. Sci. Technol.* **46**, 7454–7462 (2012).
12. Pósfai, M. et al. Atmospheric tar balls: particles from biomass and biofuel burning. *J. Geophys. Res. Atmos.* **109**, D06213 (2004).
13. Chakrabarty, R. K. et al. Brown carbon in tar balls from smoldering biomass combustion. *Atmos. Chem. Phys.* **10**, 6363–6370 (2010).
14. Sedlacek Iii, A. J. et al. Formation and evolution of tar balls from northwestern US wildfires. *Atmos. Chem. Phys.* **18**, 11289–11301 (2018).
15. Schwarz, J. et al. Measurement of the mixing state, mass, and optical size of individual black carbon particles in urban and biomass burning emissions. *Geophys. Res. Lett.* **35**, L13810 (2008).
16. Liu, D. et al. Contrasting physical properties of black carbon in urban Beijing between winter and summer. *Atmos. Chem. Phys.* **19**, 6749–6769 (2019).
17. Haslett, S. L. et al. Highly controlled, reproducible measurements of aerosol emissions from combustion of a common African biofuel source. *Atmos. Chem. Phys.* **18**, 385–403 (2018).
18. Hodgson, A. K. et al. Near-field emission profiling of tropical forest and Cerrado fires in Brazil during SAMBBA 2012. *Atmos. Chem. Phys.* **18**, 5619–5638 (2018).
19. Weingartner, E., Burtscher, H. & Baltensperger, U. Hygroscopic properties of carbon and diesel soot particles. *Atmos. Environ.* **31**, 2311–2327 (1997).
20. Saleh, R. et al. Brownness of organics in aerosols from biomass burning linked to their black carbon content. *Nat. Geosci.* **7**, 647–650 (2014).
21. Chen, Y. & Bond, T. Light absorption by organic carbon from wood combustion. *Atmos. Chem. Phys.* **10**, 1773–1787 (2010).
22. Lu, Z. et al. Light absorption properties and radiative effects of primary organic aerosol emissions. *Environ. Sci. Technol.* **49**, 4868–4877 (2015).
23. Hammer, M. S. et al. Interpreting the ultraviolet aerosol index observed with the OMI satellite instrument to understand absorption by organic aerosols: implications for atmospheric oxidation and direct radiative effects. *Atmos. Chem. Phys.* **16**, 2507–2523 (2016).
24. Sandradewi, J. et al. Using aerosol light absorption measurements for the quantitative determination of wood burning and traffic emission contributions to particulate matter. *Environ. Sci. Technol.* **42**, 3316–3323 (2008).
25. Adachi, K., Chung, S. H. & Buseck, P. R. Shapes of soot aerosol particles and implications for their effects on climate. *J. Geophys. Res. Atmos.* **115**, D15206 (2010).
26. Wang, Y. et al. Fractal dimensions and mixing structures of soot particles during atmospheric processing. *Environ. Sci. Technol. Lett.* **4**, 487–493 (2017).
27. Liu, D. et al. Size distribution, mixing state and source apportionment of black carbon aerosol in London during wintertime. *Atmos. Chem. Phys.* **14**, 10061–10084 (2014).
28. Liggio, J. et al. Are emissions of black carbon from gasoline vehicles underestimated? Insights from near and on-road measurements. *Environ. Sci. Technol.* **46**, 4819–4828 (2012).
29. Girotto, G. et al. Fractal-like tar ball aggregates from wildfire smoke. *Environ. Sci. Technol. Lett.* **5**, 360–365 (2018).
30. Lack, D. A. et al. Particulate emissions from commercial shipping: Chemical, physical, and optical properties. *J. Geophys. Res.* **114**, D00F04 (2009).
31. Corbin, J. C. et al. Infrared-absorbing carbonaceous tar can dominate light absorption by marine-engine exhaust. *npjClim. Atmos. Sci.* **2**, 12 (2019).
32. Lack, D. A., Moosmuller, H., McMeeking, G. R., Chakrabarty, R. K. & Baumgardner, D. Characterizing elemental, equivalent black, and refractory black carbon aerosol particles: a review of techniques, their limitations and uncertainties. *Anal. Bioanal. Chem.* **406**, 99–122 (2014).
33. Bond, T. C., Anderson, T. L. & Campbell, D. Calibration and intercomparison of filter-based measurements of visible light absorption by aerosols. *Aerosol Sci. Technol.* **30**, 582–600 (1999).
34. Ogren, J. A. & Charlson, R. J. Elemental carbon in the atmosphere: cycle and lifetime. *Tellus B* **35**, 241–254 (1983).
35. Weingartner, E. et al. Absorption of light by soot particles: determination of the absorption coefficient by means of aethalometers. *J. Aerosol Sci.* **34**, 1445–1463 (2003).
36. Schmid, O. et al. Spectral light absorption by ambient aerosols influenced by biomass burning in the Amazon Basin. I: comparison and field calibration of absorption measurement techniques. *Atmos. Chem. Phys.* **6**, 3443–3462 (2006).
37. Chow, J. C. et al. The DRI thermal/optical reflectance carbon analysis system: description, evaluation and applications in US air quality studies. *Atmos. Environ. Part A. Gen. Top.* **27**, 1185–1201 (1993).
38. Petzold, A. et al. Evaluation of multiangle absorption photometry for measuring aerosol light absorption. *Aerosol Sci. Technol.* **39**, 40–51 (2005).

39. Vii, A. T. B. et al. Intercomparison between NIOSH, IMPROVE_A, and EUSAAR_2 protocols: finding an optimal thermal-optical protocol for Philippines OC/EC samples. *Atmos. Pollut. Res.* **6**, 334–342 (2015).
40. Turpin, B. J., Saxena, P. & Andrews, E. Measuring and simulating particulate organics in the atmosphere: problems and prospects. *Atmos. Environ.* **34**, 2983–3013 (2000).
41. Lack, D. A., Lovejoy, E. R., Baynard, T., Pettersson, A. & Ravishankara, A. R. Aerosol absorption measurement using photoacoustic spectroscopy: sensitivity, calibration, and uncertainty developments. *Aerosol Sci. Technol.* **40**, 697–708 (2006).
42. Sedlacek, A. J., Lewis, E. R., Kleinman, L., Xu, J. & Zhang, Q. Determination of and evidence for non-core-shell structure of particles containing black carbon using the Single-Particle Soot Photometer (SP2). *Geophys. Res. Lett.* **39**, L06802 (2012).
43. Radney, J. G. & Zangmeister, C. D. Measurement of Gas and Aerosol Phase Absorption Spectra across the Visible and Near-IR Using Supercontinuum Photoacoustic Spectroscopy. *Anal. Chem.* **87**, 7356–7363 (2015).
44. Lack, D. A. et al. Aircraft instrument for comprehensive characterization of aerosol optical properties, part 2: black and brown carbon absorption and absorption enhancement measured with photo acoustic spectroscopy. *Aerosol Sci. Technol.* **46**, 555–568 (2012).
45. Onasch, T. B. et al. Single scattering Albedo monitor for airborne particulates. *Aerosol Sci. Technol.* **49**, 267–279 (2015).
46. Liu, D. et al. The effect of complex black carbon microphysics on the determination of the optical properties of brown carbon. *Geophys. Res. Lett.* **42**, 613–619 (2015).
47. Koch, D. et al. Evaluation of black carbon estimations in global aerosol models. *Atmos. Chem. Phys.* **9**, 9001–9026 (2009).
48. Petzold, A. et al. Recommendations for reporting" black carbon" measurements. *Atmos. Chem. Phys.* **13**, 8365–8379 (2013).
49. Quay, B., Lee, T. W., Ni, T. & Santoro, R. J. Spatially resolved measurements of soot volume fraction using laser-induced incandescence. *Combust. Flame* **97**, 384–392 (1994).
50. Stephens, M., Turner, N. C. & Sandberg, J. C. Particle identification by laser-induced incandescence in a solid-state laser cavity. *Appl. Opt.* **42**, 3726–3736 (2003).
51. Schwarz, J. et al. Single-particle measurements of midlatitude black carbon and light-scattering aerosols from the boundary layer to the lower stratosphere. *J. Geophys. Res. Atmos.* **111,** D16207 (2006).
52. Moteki, N. & Kondo, Y. Effects of mixing state on black carbon measurements by laser-induced incandescence. *Aerosol Sci. Technol.* **41**, 398–417 (2007).
53. Liu, D. et al. Single particle characterization of black carbon aerosols at a tropospheric alpine site in Switzerland. *Atmos. Chem. Phys.* **10**, 7389–7407 (2010).
54. Kondo, Y. et al. Consistency and traceability of black carbon measurements made by laser-induced incandescence, thermal-optical transmittance, and filter-based photo-absorption techniques. *Aerosol Sci. Technol.* **45**, 295–312 (2011).
55. Moteki, N. & Kondo, Y. Dependence of laser-induced incandescence on physical properties of black carbon aerosols: measurements and theoretical interpretation. *Aerosol Sci. Technol.* **44**, 663–675 (2010).
56. Gao, R. et al. A novel method for estimating light-scattering properties of soot aerosols using a modified single-particle soot photometer. *Aerosol Sci. Technol.* **41**, 125–135 (2007).
57. Schwarz, J. P. et al. The detection efficiency of the single particle soot photometer. *Aerosol Sci. Technol.* **44**, 612–628 (2010).
58. Schwarz, J. P. et al. Assessing single particle soot photometer and integrating sphere/integrating sandwich spectrophotometer measurement techniques for quantifying black carbon concentration in snow. *Atmos. Meas. Technol.* **5**, 2581–2592 (2012).
59. Ohata, S., Moteki, N., Schwarz, J., Fahey, D. & Kondo, Y. Evaluation of a method to measure black carbon particles suspended in rainwater and snow samples. *Aerosol Sci. Technol.* **47**, 1073–1082 (2013).
60. Onasch, T. et al. Soot particle aerosol mass spectrometer: development, validation, and initial application. *Aerosol Sci. Technol.* **46**, 804–817 (2012).
61. Weinzierl, B. B. *Radiatively-Driven Processes in Forest Fire and Desert Dust Plumes* (lmu, 2008).
62. Koch, D. & Del Genio, A. Black carbon semi-direct effects on cloud cover: review and synthesis. *Atmos. Chem. Phys.* **10**, 7685–7696 (2010).
63. Liu, D. et al. Efficient vertical transport of black carbon in the planetary boundary layer. *Geophys. Res. Lett.* **47**, e2020GL088858 (2020).
64. Ding, A. et al. Enhanced haze pollution by black carbon in megacities in China. *Geophys. Res. Lett.* **43**, 2873–2879 (2016).
65. Liu, D. et al. Enhanced heating rate of black carbon above planetary boundary layer over megacities in summertime. *Environ. Res. Lett.* https://doi.org/10.1088/1748-9326/ab4872 (2019).
66. Zhao, D. et al. Vertical evolution of black carbon characteristics and heating rate during a haze event in Beijing winter. *Sci. Tot. Environ.* **709**, 136251 (2020).
67. Li, Z. et al. Aerosol and boundary-layer interactions and impact on air quality. *Natl Sci. Rev.* **4**, 810–833 (2017).
68. Haywood, J. & Boucher, O. Estimates of the direct and indirect radiative forcing due to tropospheric aerosols: a review. *Rev. Geophys.* **38**, 513–543 (2000).
69. Samset, B. H. & Myhre, G. Vertical dependence of black carbon, sulphate and biomass burning aerosol radiative forcing. *Geophys. Res. Lett.* **38**, L24802 (2011).
70. Gordon, M. et al. Determining air pollutant emission rates based on mass balance using airborne measurement data over the Alberta oil sands operations. *Atmos. Meas. Technol.* **8**, 3745–3765 (2015).
71. Yu, P. et al. Black carbon lofts wildfire smoke high into the stratosphere to form a persistent plume. *Science* **365**, 587–590 (2019).
72. Zhang, Y. et al. Top-of-atmosphere radiative forcing affected by brown carbon in the upper troposphere. *Nat. Geosci.* **10**, 486–489 (2017).
73. Ban-Weiss, G. A., Cao, L., Bala, G. & Caldeira, K. Dependence of climate forcing and response on the altitude of black carbon aerosols. *Clim. Dyn.* **38**, 897–911 (2012).
74. Moteki, N. et al. Evolution of mixing state of black carbon particles: aircraft measurements over the western Pacific in March 2004. *Geophys. Res. Lett.* **34**, 11803 (2007).
75. Akagi, S. et al. Evolution of trace gases and particles emitted by a chaparral fire in California. *Atmos. Chem. Phys.* **12**, 1397–1421 (2012).
76. Moffet, R. C. et al. Morphology and mixing of black carbon particles collected in central California during the CARES field study. *Atmos. Chem. Phys.* **16**, 14515–14525 (2016).
77. Shen, Z. et al. Analysis of transpacific transport of black carbon during HIPPO-3: implications for black carbon aging. *Atmos. Chem. Phys.* **14**, 6315–6327 (2014).
78. He, C. et al. Microphysics-based black carbon aging in a global CTM: constraints from HIPPO observations and implications for global black carbon budget. *Atmos. Chem. Phys.* **16**, 3077–3098 (2016).
79. Jacobson, M. Z. Strong radiative heating due to the mixing state of black carbon in atmospheric aerosols. *Nature* **409**, 695–697 (2001).
80. Zhang, R. et al. Variability in morphology, hygroscopicity, and optical properties of soot aerosols during atmospheric processing. *Proc. Natl Acad. Sci. USA* **105**, 10291 (2008).
81. Liu, D. et al. Black-carbon absorption enhancement in the atmosphere determined by particle mixing state. *Nat. Geosci.* **10**, 184–188 (2017).
82. Peng, J. et al. Markedly enhanced absorption and direct radiative forcing of black carbon under polluted urban environments. *Proc. Natl. Acad. Sci. USA* **113**, 4266–4271 (2016).
83. Cappa, C. D. et al. Radiative absorption enhancements due to the mixing state of atmospheric black carbon. *Science* **337**, 1078–1081 (2012).
84. He, C. *Springer Series in Light Scattering Springer Series in Light Scattering* Ch. 5, 219–254 (Springer, 2019).
85. Li, C. et al. Re-evaluating black carbon in the Himalayas and the Tibetan Plateau: concentrations and deposition. *Atmos. Chem. Phys.* **17**, 11899–11912 (2017).
86. He, C. et al. Variation of the radiative properties during black carbon aging: theoretical and experimental intercomparison. *Atmos. Chem. Phys.* **15**, 11967–11980 (2015).
87. He, C. et al. Intercomparison of the GOS approach, superposition T-matrix method, and laboratory measurements for black carbon optical properties during aging. *J. Quant. Spectrosc. Ra.* **184**, 287–296 (2016).
88. Möhler, O. et al. Effect of sulfuric acid coating on heterogeneous ice nucleation by soot aerosol particles. *J. Geophys. Res. Atmos.* **110**, D11210 (2005).
89. Riemer, N., Ault, A. P., West, M., Craig, R. L. & Curtis, J. H. Aerosol mixing state: measurements, modeling, and impacts. *Rev. Geophys.* **57**, 187–249 (2019).
90. Matsui, H., Koike, M., Kondo, Y., Fast, J. D. & Takigawa, M. Development of an aerosol microphysical module: aerosol two-dimensional bin module for foRmation and Aging Simulation (ATRAS). *Atmos. Chem. Phys.* **14**, 10315–10331 (2014).
91. Riemer, N., West, M., Zaveri, R. A. & Easter, R. C. Simulating the evolution of soot mixing state with a particle-resolved aerosol model. *J. Geophys. Res. Atmos.* **114**, D09202 (2009).
92. Fierce, L., Bond, T. C., Bauer, S. E., Mena, F. & Riemer, N. Black carbon absorption at the global scale is affected by particle-scale diversity in composition. *Nat. Commun.* **7**, 12361 (2016).
93. Ching, J., Fast, J., West, M. & Riemer, N. Metrics to quantify the importance of mixing state for CCN activity. *Atmos. Chem. Phys.* **17**, 7445–7458 (2017).
94. Schwarz, J. P. et al. Global-scale seasonally resolved black carbon vertical profiles over the Pacific. *Geophys. Res. Lett.* **40**, 5542–5547 (2013).
95. Wang, X. et al. Exploiting simultaneous observational constraints on mass and absorption to estimate the global direct radiative forcing of black carbon and brown carbon. *Atmos. Chem. Phys.* **14**, 10989–11010 (2014).
96. Matsui, H., Hamilton, D. S. & Mahowald, N. M. Black carbon radiative effects highly sensitive to emitted particle size when resolving mixing-state diversity. *Nat. Commun.* **9**, 3446 (2018).
97. Pöschl, U., Letzel, T., Schauer, C. & Niessner, R. Interaction of ozone and water vapor with spark discharge soot aerosol particles coated with benzo[a]pyrene:

O3 and H2O adsorption, benzo[a]pyrene degradation, and atmospheric implications. *J. Phys. Chem. A* **105**, 4029–4041 (2001).
98. Lee, H. J., Aiona, P. K., Laskin, A., Laskin, J. & Nizkorodov, S. A. Effect of solar radiation on the optical properties and molecular composition of laboratory proxies of atmospheric brown carbon. *Environ. Sci. Technol.* **48**, 10217–10226 (2014).
99. Zhao, R. et al. Photochemical processing of aqueous atmospheric brown carbon. *Atmos. Chem. Phys.* **15**, 6087–6100 (2015).
100. Forrister, H. et al. Evolution of brown carbon in wildfire plumes. *Geophys. Res. Lett.* **42**, 4623–4630 (2015).
101. Wong, J. P. S., Nenes, A. & Weber, R. J. Changes in light absorptivity of molecular weight separated brown carbon due to photolytic aging. *Environ. Sci. Technol.* **51**, 8414–8421 (2017).
102. Smith, J. D., Sio, V., Yu, L., Zhang, Q. & Anastasio, C. Secondary organic aerosol production from aqueous reactions of atmospheric phenols with an organic triplet excited state. *Environ. Sci. Technol.* **48**, 1049–1057 (2014).
103. Lambe, A. T. et al. Relationship between oxidation level and optical properties of secondary organic aerosol. *Environ. Sci. Technol.* **47**, 6349–6357 (2013).
104. Jacobson, M. Z. Isolating nitrated and aromatic aerosols and nitrated aromatic gases as sources of ultraviolet light absorption. *J. Geophys. Res. Atmos.* **104**, 3527–3542 (1999).
105. Updyke, K. M., Nguyen, T. B. & Nizkorodov, S. A. Formation of brown carbon via reactions of ammonia with secondary organic aerosols from biogenic and anthropogenic precursors. *Atmos. Environ.* **63**, 22–31 (2012).
106. Hoffer, A. et al. Optical properties of humic-like substances (HULIS) in biomass-burning aerosols. *Atmos. Chem. Phys.* **6**, 3563–3570 (2006).
107. Keyte, I. J., Harrison, R. M. & Lammel, G. Chemical reactivity and long-range transport potential of polycyclic aromatic hydrocarbons—a review. *Chem. Soc. Rev.* **42**, 9333–9391 (2013).
108. Liu, P. F. et al. Ultraviolet and visible complex refractive indices of secondary organic material produced by photooxidation of the aromatic compounds toluene and m-xylene. *Atmos. Chem. Phys.* **15**, 1435–1446 (2015).
109. Lang-Yona, N. et al. Interaction of internally mixed aerosols with light. *Phys. Chem. Chem. Phys.* **12**, 21–31 (2010).
110. Liu, P. et al. Highly viscous states affect the browning of atmospheric organic particulate matter. *ACS Cent. Sci.* **4**, 207–215 (2018).
111. Feng, Y., Ramanathan, V. & Kotamarthi, V. R. Brown carbon: a significant atmospheric absorber of solar radiation? *Atmos. Chem. Phys.* **13**, 8607–8621 (2013).
112. Yan, C. et al. Important fossil source contribution to brown carbon in Beijing during winter. *Sci. Rep.* **7**, 43182–43182 (2017).
113. Jo, D. S., Park, R. J., Lee, S., Kim, S. W. & Zhang, X. A global simulation of brown carbon: implications for photochemistry and direct radiative effect. *Atmos. Chem. Phys.* **16**, 3413–3432 (2016).
114. Wang, X. et al. Exploring the observational constraints on the simulation of brown carbon. *Atmos. Chem. Phys.* **18**, 635–653 (2018).
115. Zhang, A. et al. Modeling global radiative effect of brown carbon: a larger heating source in the tropical free troposphere than black carbon. *Atmos. Chem. Phys. Discuss.* **2019**, 1–36 (2019).
116. Wang, X. et al. Deriving brown carbon from multiwavelength absorption measurements: method and application to AERONET and Aethalometer observations. *Atmos. Chem. Phys.* **16**, 12733–12752 (2016).
117. Brown, H. et al. Radiative effect and climate impacts of brown carbon with the Community Atmosphere Model (CAM5). *Atmos. Chem. Phys.* **18**, 17745–17768 (2018).
118. Saleh, R. et al. Contribution of brown carbon and lensing to the direct radiative effect of carbonaceous aerosols from biomass and biofuel burning emissions. *J. Geophys. Res. Atmos.* **120**, 10,285–210,296 (2015).
119. Bahadur, R., Praveen, P. S., Xu, Y. & Ramanathan, V. Solar absorption by elemental and brown carbon determined from spectral observations. *Proc. Natl Acad. Sci. USA* **109**, 17366–17371 (2012).
120. Liu, J. et al. Size-resolved measurements of brown carbon in water and methanol extracts and estimates of their contribution to ambient fine-particle light absorption. *Atmos. Chem. Phys.* **13**, 12389–12404 (2013).
121. Shetty, N. J., Pandey, A., Baker, S., Hao, W. M. & Chakrabarty, R. K. Measuring light absorption by freshly emitted organic aerosols: optical artifacts in traditional solvent-extraction-based methods. *Atmos. Chem. Phys.* **19**, 8817–8830 (2019).
122. Dusek, U. et al. Size matters more than chemistry for cloud-nucleating ability of aerosol particles. *Science* **312**, 1375–1378 (2006).
123. Seinfeld, J. H. & Pandis, S. N. *Atmospheric Chemistry and Physics: From Air Pollution to Climate Change* (John Wiley & Sons, 2012).
124. Jacobson, M. Z. Investigating cloud absorption effects: Global absorption properties of black carbon, tar balls, and soil dust in clouds and aerosols. *J. Geophys. Res. Atmos.* **117**, D06205 (2012).
125. Duplissy, J. et al. Relating hygroscopicity and composition of organic aerosol particulate matter. *Atmos. Chem. Phys.* **11**, 1155–1165 (2011).
126. McMeeking, G., Good, N., Petters, M., McFiggans, G. & Coe, H. Influences on the fraction of hydrophobic and hydrophilic black carbon in the atmosphere. *Atmos. Chem. Phys.* **11**, 5099–5112 (2011).
127. Liu, D. et al. Ambient black carbon particle hygroscopic properties controlled by mixing state and composition. *Atmos. Chem. Phys.* **13**, 2015–2029 (2013).
128. Schwarz, J. P. et al. Technique and theoretical approach for quantifying the hygroscopicity of black-carbon-containing aerosol using a single particle soot photometer. *J. Aerosol Sci.* **81**, 110–126 (2015).
129. Ohata, S. et al. Hygroscopicity of materials internally mixed with black carbon measured in Tokyo. *J. Geophys. Res. Atmos.* **121**, 362–381 (2016).
130. Wu, Y. et al. Characterization of size-resolved hygroscopicity of black carbon-containing particle in urban environment. *Environ. Sci. Technol.* **53**, 14212–14221 (2019).
131. Kuwata, M., Kondo, Y., Mochida, M., Takegawa, N. & Kawamura, K. Dependence of CCN activity of less volatile particles on the amount of coating observed in Tokyo. *J. Geophys. Res. Atmos.* **112**, D11207 (2007).
132. Ding, S. et al. Size-related physical properties of black carbon in the lower atmosphere over Beijing and Europe. *Environ. Sci. Technol.* **53**, 11112–11121 (2019).
133. Rissler, J. et al. Physical properties of the sub-micrometer aerosol over the Amazon rain forest during the wet-to-dry season transition? Comparison of modeled and measured CCN concentrations. *Atmos. Chem. Phys.* **4**, 2119–2143 (2004).
134. Roberts, G. C., Nenes, A., Seinfeld, J. H. & Andreae, M. O. Impact of biomass burning on cloud properties in the Amazon Basin. *J. Geophys. Res.* **108**, 4062 (2003).
135. Canagaratna, M. R. et al. Elemental ratio measurements of organic compounds using aerosol mass spectrometry: characterization, improved calibration, and implications. *Atmos. Chem. Phys.* **15**, 253–272 (2015).
136. Massoli, P. et al. Relationship between aerosol oxidation level and hygroscopic properties of laboratory generated secondary organic aerosol (SOA) particles. *Geophys. Res. Lett.* **37**, L24801 (2010).
137. Frosch, M. et al. Relating cloud condensation nuclei activity and oxidation level of α-pinene secondary organic aerosols. *J. Geophys. Res. Atmos.* **116**, D22212 (2011).
138. Decesari, S. et al. Characterization of the organic composition of aerosols from Rondônia, Brazil, during the LBA-SMOCC 2002 experiment and its representation through model compounds. *Atmos. Chem. Phys.* **6**, 375–402 (2006).
139. Lin, Y.-H. et al. Light-absorbing oligomer formation in secondary organic aerosol from reactive uptake of isoprene epoxydiols. *Environ. Sci. Technol.* **48**, 12012–12021 (2014).
140. Rincón, A. G., Guzmán, M. I., Hoffmann, M. R. & Colussi, A. J. Optical absorptivity versus molecular composition of model organic aerosol matter. *J. Phys. Chem. A* **113**, 10512–10520 (2009).
141. You, Y. et al. Images reveal that atmospheric particles can undergo liquid-liquid phase separations. *Proc. Natl Acad. Sci. USA* **109**, 13188–13193 (2012).
142. Ruehl, C. R., Davies, J. F. & Wilson, K. R. An interfacial mechanism for cloud droplet formation on organic aerosols. *Science* **351**, 1447–1450 (2016).
143. Ovadnevaite, J. et al. Surface tension prevails over solute effect in organic-influenced cloud droplet activation. *Nature* **546**, 637–641 (2017).
144. Kärcher, B., Möhler, O., DeMott, P. J., Pechtl, S. & Yu, F. Insights into the role of soot aerosols in cirrus cloud formation. *Atmos. Chem. Phys.* **7**, 4203–4227 (2007).
145. Möhler, O. et al. Ice nucleation on flame soot aerosol of different organic carbon content. *Meteorol. Z.* **14**, 477–484 (2005).
146. Levin, E. J. T. et al. A new method to determine the number concentrations of refractory black carbon ice nucleating particles. *Aerosol Sci. Tech.* **48**, 1264–1275 (2014).
147. Fornea, A. P., Brooks, S. D., Dooley, J. B. & Saha, A. Heterogeneous freezing of ice on atmospheric aerosols containing ash, soot, and soil. *J. Geophys. Res. Atmos.* **114**, D13201 (2009).
148. Crawford, I. et al. Studies of propane flame soot acting as heterogeneous ice nuclei in conjunction with single particle soot photometer measurements. *Atmos. Chem. Phys.* **11**, 9549–9561 (2011).
149. Ullrich, R. et al. A new ice nucleation active site parameterization for desert dust and soot. *J. Atmos. Sci.* **74**, 699–717 (2017).
150. Kanji, Z. A. et al. Overview of ice nucleating particles. *Meteorol. Monogr.* **58**, 1.1–1.33 (2017).
151. Chen, J. et al. Ice-nucleating particle concentrations unaffected by urban air pollution in Beijing, China. *Atmos. Chem. Phys.* **18**, 3523–3539 (2018).
152. Kulkarni, G. et al. Ice nucleation activity of diesel soot particles at cirrus relevant temperature conditions: effects of hydration, secondary organics coating, soot morphology, and coagulation. *Geophys. Res. Lett.* **43**, 3580–3588 (2016).

153. Knopf, D. A., Alpert, P. A. & Wang, B. The role of organic aerosol in atmospheric ice nucleation: a review. *Acs. Earth. Space Chem.* **2**, 168–202 (2018).
154. Berkemeier, T., Shiraiwa, M., Pöschl, U. & Koop, T. Competition between water uptake and ice nucleation by glassy organic aerosol particles. *Atmos. Chem. Phys.* **14**, 12513–12531 (2014).
155. Shiraiwa, M. et al. Global distribution of particle phase state in atmospheric secondary organic aerosols. *Nat. Commun.* **8**, 15002 (2017).
156. Wang, B. & Knopf, D. A. Heterogeneous ice nucleation on particles composed of humic-like substances impacted by O3. *J. Geophys. Res. Atmos.* **116**, D03205 (2011).
157. Kärcher, B., Hendricks, J. & Lohmann, U. Physically based parameterization of cirrus cloud formation for use in global atmospheric models. *J. Geophys. Res. Atmos.* **111**, D01205 (2006).
158. Lee, D. S. et al. Transport impacts on atmosphere and climate: aviation. *Atmos. Environ.* **44**, 4678–4734 (2010).
159. Jacobson, M. Z., Wilkerson, J. T., Naiman, A. D. & Lele, S. K. The effects of aircraft on climate and pollution. Part II: 20-year impacts of exhaust from all commercial aircraft worldwide treated individually at the subgrid scale. *Faraday Discuss.* **165**, 369–382 (2013).
160. Verheggen, B. et al. Aerosol partitioning between the interstitial and the condensed phase in mixed-phase clouds. *J. Geophys. Res. Atmos.* **112**, D23202 (2007).
161. Ding, S. et al. Observed interactions between black carbon and hydrometeor during wet scavenging in mixed-phase clouds. *Geophys. Res. Lett.* https://doi.org/10.1029/2019gl083171 (2019).
162. Facchini, M. C. et al. Partitioning of the organic aerosol component between fog droplets and interstitial air. *J. Geophys. Res. Atmos.* **104**, 26821–26832 (1999).
163. Motos, G. et al. Droplet activation behaviour of atmospheric black carbon particles in fog as a function of their size and mixing state. *Atmos. Chem. Phys.* **19**, 2183–2207 (2019).
164. Cziczo, D. J., Murphy, D. M., Hudson, P. K. & Thomson, D. S. Single particle measurements of the chemical composition of cirrus ice residue during CRYSTAL-FACE. *J. Geophys. Res. Atmos.* **109**, D04201 (2004).
165. Baumgardner, D., Subramanian, R., Twohy, C., Stith, J. & Kok, G. Scavenging of black carbon by ice crystals over the northern Pacific. *Geophys. Res. Lett.* **35**, L22815 (2008).
166. Cozic, J. et al. Scavenging of black carbon in mixed phase clouds at the high alpine site Jungfraujoch. *Atmos. Chem. Phys.* **7**, 1797–1807 (2007).
167. Twohy, C. H. et al. Saharan dust particles nucleate droplets in eastern Atlantic clouds. *Geophys. Res. Lett.* **36**, L01807 (2009).
168. Zhang, G. et al. The single-particle mixing state and cloud scavenging of black carbon: a case study at a high-altitude mountain site in southern China. *Atmos. Chem. Phys.* **17**, 14975–14985 (2017).
169. Muhlbauer, A. & Lohmann, U. Sensitivity studies of the role of aerosols in warm-phase orographic precipitation in different dynamical flow regimes. *J. Atmos. Sci.* **65**, 2522–2542 (2008).
170. Heintzenberg, J. & Leck, C. Seasonal variation of the atmospheric aerosol near the top of the marine boundary layer over Spitsbergen related to the Arctic sulphur cycle. *Tellus B Chem. Phys. Meteorol.* **46**, 52–67 (1994).
171. Qi, L., Li, Q., Li, Y. & He, C. Factors controlling black carbon distribution in the Arctic. *Atmos. Chem. Phys.* **17**, 1037–1059 (2017).
172. Fan, S. M. et al. Inferring ice formation processes from global-scale black carbon profiles observed in the remote atmosphere and model simulations. *J. Geophys. Res. Atmos.* **117**, D23205 (2012).
173. Liu, L. & Mishchenko, M. I. Optics of water microdroplets with soot inclusions: exact versus approximate results. *J. Quant. Spectrosc. Radiat. Transfer* **178**, 255–262 (2016).
174. Chýlek, P. et al. Black carbon and absorption of solar radiation by clouds. *J. Geophys. Res. Atmos.* **101**, 23365–23371 (1996).
175. Liou, K. N., Takano, Y., Yue, Q. & Yang, P. On the radiative forcing of contrail cirrus contaminated by black carbon. *Geophys. Res. Lett.* **40**, 778–784 (2013).
176. Ekman, A. M. L., Wang, C., Wilson, J. & Ström, J. Explicit simulations of aerosol physics in a cloud-resolving model: a sensitivity study based on an observed convective cloud. *Atmos. Chem. Phys.* **4**, 773–791 (2004).
177. Wang, X., Zhang, L. & Moran, M. D. Uncertainty assessment of current size-resolved parameterizations for below-cloud particle scavenging by rain. *Atmos. Chem. Phys.* **10**, 5685–5705 (2010).
178. Ohata, S., Moteki, N., Mori, T., Koike, M. & Kondo, Y. A key process controlling the wet removal of aerosols: new observational evidence. *Sci. Rep.* **6**, 34113 (2016).
179. Herckes, P., Valsaraj, K. T. & Collett, J. L. A review of observations of organic matter in fogs and clouds: origin, processing and fate. *Atmos. Res.* **132-133**, 434–449 (2013).
180. Yang, Y. et al. Recent advances in quantifying wet scavenging efficiency of black carbon aerosol. *Atmosphere* **10**, 175 (2019).
181. Torres, A., Bond, T. C., Lehmann, C. M. B., Subramanian, R. & Hadley, O. L. Measuring organic carbon and black carbon in rainwater: evaluation of methods. *Aerosol Sci. Technol.* **48**, 239–250 (2014).
182. Mori, T. et al. Wet deposition of black carbon at a remote site in the East China Sea. *J. Geophys. Res. Atmos.* **119**, 10485–10498 (2014).
183. Gelencsér, A. et al. In-situ formation of light-absorbing organic matter in cloud water. *J. Atmos. Chem.* **45**, 25–33 (2003).
184. Zarzana, K. J., De Haan, D. O., Freedman, M. A., Hasenkopf, C. A. & Tolbert, M. A. Optical properties of the products of α-dicarbonyl and amine reactions in simulated cloud droplets. *Environ. Sci. Technol.* **46**, 4845–4851 (2012).
185. Liu, D. et al. The importance of Asia as a source of black carbon to the European Arctic during springtime 2013. *Atmos. Chem. Phys.* **15**, 11537–11555 (2015).
186. Kanaya, Y. et al. Long-term observations of black carbon mass concentrations at Fukue Island, western Japan, during 2009–2015: constraining wet removal rates andemission strengths from East Asia. *Atmos. Chem. Phys.* **16**, 10689–10705 (2016).
187. Kondo, Y. et al. Effects of wet deposition on the abundance and size distribution of black carbon in East Asia. *J. Geophys. Res. Atmos.* **121**, 4691–4712 (2016).
188. Liu, H., Jacob, D. J., Bey, I. & Yantosca, R. M. Constraints from 210Pb and 7Be on wet deposition and transport in a global three-dimensional chemical tracer model driven by assimilated meteorological fields. *J. Geophys. Res.* **106**, 12109–12128 (2001).
189. Liu, J., Fan, S., Horowitz, L. W. & Levy, H. Evaluation of factors controlling long-range transport of black carbon to the Arctic. *J. Geophys. Res. Atmos.* **116**, D04307 (2011).
190. Wang, Q. et al. Global budget and radiative forcing of black carbon aerosol: constraints from pole-to-pole (HIPPO) observations across the Pacific. *J. Geophys. Res. Atmos.* **119**, 195–206 (2014).
191. Lund, M. T. et al. Short black carbon lifetime inferred from a global set of aircraft observations. *npjClim. Atmos. Sci.* **1**, 31 (2018).
192. Qi, L., Li, Q., He, C., Wang, X. & Huang, J. Effects of the Wegener–Bergeron–Findeisen process on global black carbon distribution. *Atmos. Chem. Phys.* **17**, 7459–7479 (2017).
193. Liu, X., Penner, J. E. & Wang, M. Influence of anthropogenic sulfate and black carbon on upper tropospheric clouds in the NCAR CAM3 model coupled to the IMPACT global aerosol model. *J. Geophys. Res. Atmos.* **114**, D03204 (2009).
194. Gettelman, A., Liu, X., Barahona, D., Lohmann, U. & Chen, C. Climate impacts of ice nucleation. *J. Geophys. Res. Atmos.* **117**, D20201 (2012).
195. Eckhardt, S. et al. Current model capabilities for simulating black carbon and sulfate concentrations in the Arctic atmosphere: a multi-model evaluation using a comprehensive measurement data set. *Atmos. Chem. Phys.* **15**, 9413–9433 (2015).
196. Emerson, E. W., Katich, J. M., Schwarz, J. P., McMeeking, G. R. & Farmer, D. K. Direct measurements of dry and wet deposition of black carbon over a grassland. *J. Geophys. Res. Atmos.* **123**, 277–212, 290 (2018).
197. Wesely, M. L. Parameterization of surface resistances to gaseous dry deposition in regional-scale numerical models. *Atmos. Environ.* **23**, 1293–1304 (1989).
198. Zhang, L., Gong, S. L., Padro, J. & Barrie, L. A size-segregated particle dry deposition scheme for an atmospheric aerosol module. *Atmos. Environ.* **35**, 549–560 (2001).
199. Petroff, A. & Zhang, L. Development and validation of a size-resolved particle dry deposition scheme for application in aerosol transport models. *Geosci. Model Dev.* **3**, 753–769 (2010).
200. Wu, M. et al. Impacts of aerosol dry deposition on black carbon spatial distributions and radiative effects in the community atmosphere model CAM5. *J. Adv. Model. Earth. Syst.* **10**, 1150–1171 (2018).
201. Jacobson, M. Z. Climate response of fossil fuel and biofuel soot, accounting for soot's feedback to snow and sea ice albedo and emissivity. *J. Geophys. Res.* **109**, D14203 (2004).
202. Qian, Y. et al. Light-absorbing particles in snow and ice: Measurement and modeling of climatic and hydrological impact. *Adv. Atmos. Sci.* **32**, 64–91 (2015).
203. He, C. & Flanner, M. *Springer Series in Light Scattering Springer Series in Light Scattering* Ch. 3, 67–133 (Springer, 2020).
204. Skiles, S. M., Flanner, M., Cook, J. M., Dumont, M. & Painter, T. H. Radiative forcing by light-absorbing particles in snow. *Nat. Clim. Change* **8**, 964–971 (2018).
205. Hansen, J. & Nazarenko, L. Soot climate forcing via snow and ice albedos. *Proc. Nat. Acad. Sci. USA* **101**, 423–428 (2004).
206. Flanner, M. G., Zender, C. S., Randerson, J. T. & Rasch, P. J. Present-day climate forcing and response from black carbon in snow. *J. Geophys. Res. Atmos.* **112**, D11202 (2007).
207. Dang, C. et al. Measurements of light-absorbing particles in snow across the Arctic, North America, and China: effects on surface albedo. *J. Geophys. Res. Atmos.* **122**, 10149–10168 (2017).
208. He, C. et al. Impact of grain shape and multiple black carbon internal mixing on snow albedo: parameterization and radiative effect analysis. *J. Geophys. Res.* **123**, 1253–1268 (2018).

209. Schwarz, J. P., Gao, R. S., Perring, A. E., Spackman, J. R. & Fahey, D. W. Black carbon aerosol size in snow. *Sci. Rep.* **3**, 1356 (2013).
210. He, C., Liou, K. N. & Takano, Y. Resolving size distribution of black carbon internally mixed with snow: impact on snow optical properties and Albedo. *Geophys. Res. Lett.* **45**, 2697–2705 (2018).
211. Zhang, Y. et al. Dissolved organic carbon in snow cover of the Chinese Altai Mountains, Central Asia: concentrations, sources and light-absorption properties. *Sci. Tot. Environ.* **647**, 1385–1397 (2019).
212. Kuchiki, K. et al. Elemental carbon, organic carbon, and dust concentrations in snow measured with thermal optical and gravimetric methods: Variations during the 2007–2013 winters at Sapporo, Japan. *J. Geophys. Res. Atmos.* **120**, 868–882 (2015).
213. Doherty, S. J., Warren, S. G., Grenfell, T. C., Clarke, A. D. & Brandt, R. E. Light-absorbing impurities in Arctic snow. *Atmos. Chem. Phys.* **10**, 11647–11680 (2010).
214. Dang, C. & Hegg, D. A. Quantifying light absorption by organic carbon in Western North American snow by serial chemical extractions. *J. Geophys. Res. Atmos.* **119**, 10,247–210,261 (2014).
215. Beres, N. D., Sengupta, D., Samburova, V., Khlystov, A. Y. & Moosmüller, H. Deposition of brown carbon onto snow: changes of snow optical and radiative properties. *Atmos. Chem. Phys. Discuss.* **2019**, 1–35 (2019).
216. Domine, F. et al. Snow physics as relevant to snow photochemistry. *Atmos. Chem. Phys.* **8**, 171–208 (2008).
217. Grannas, A. M. et al. An overview of snow photochemistry: evidence, mechanisms and impacts. *Atmos. Chem. Phys.* **7**, 4329–4373 (2007).
218. Yan, F. et al. Deposition of organic and black carbon: direct measurements at three remote stations in the Himalayas and Tibetan Plateau. *J. Geophys. Res. Atmos* **124**, 9702–9715 (2019).
219. Reddington, C. et al. The Global Aerosol Synthesis and Science Project (GASSP): measurements and modelling to reduce uncertainty. *Bull. Am. Meteorol. Soc*. **98**, 1857–1877 (2017).
220. Park, R. J., Kim, M. J., Jeong, J. I., Youn, D. & Kim, S. W. A contribution of brown carbon aerosol to the aerosol light absorption and its radiativeforcing in East Asia. *Atmos. Environ.* **44**, 1414–1421 (2010).
221. Alexander, D. T. L., Crozier, P. A. & Anderson, J. R. Brown Carbon Spheres in East Asian Outflow and Their Optical Properties. *Science* **321**, 833 (2008).
222. Kirchstetter, T. W., Novakov, T. & Hobbs, P. V. Evidence that the spectral dependence of light absorption by aerosols is affected by organiccarbon. *J. Geophys. Res.* **109**, D21208 (2004).
223. Lin, G., Penner, J. E., Flanner, M. G., Sillman, S., Xu, L. & Zhou, C. Radiative forcing of organic aerosol in the atmosphere and on snow: Effects ofSOA and brown carbon. *J. Geophys. Res.* **119**, 7453–7476 (2014).
224. Jacobson, M. Z. Effects of biomass burning on climate, accounting for heat and moisture fluxes, black and brown carbon, and cloud absorptioneffects. *J. Geophys. Res. - Atmos.* **119**, 8980–9002 (2014).
225. Zhang, X. L., Lin, Y. H., Surratt, J. D. & Weber, R. J. Sources, Composition and Absorption Ångström Exponent of Light absorbing OrganicComponents in Aerosol Extracts from the Los Angeles Basin. *Environ. Sci. Technol.* **47**, 3685–3693 (2013).
226. Wang, Q. et al. Physicochemical characteristics of black carbon aerosoland its radiative impact in a polluted urban area of China. *J. Geophys. Res. - Atmos.* **121** (2016).
227. Nakayama, T. Y. et al. Laboratory studies on optical properties of secondary organic aerosols generated during the photooxidation of toluene and the ozonolysis of *α*-pinene. *J. Geophys. Res.* **115**, D24204 (2010).

ACKNOWLEDGEMENTS

D. L. acknowledges the support from the National Key Research and Development Program of China (2016YFA0602001), the National Natural Science Foundation of China (41875167), and the Hundred Talents Program of Zhejiang University (188020*194221903/011/002).

AUTHOR CONTRIBUTIONS

D.L. proposed the study and led the writing, C.H. wrote the sections of aging of BC, modeling on LAC wet deposition, deposition of LACs in the cryosphere; J.S. wrote the sections of transport of LACs and dry deposition; X.W. wrote the sections of aging of BrC and modeling of BrC. All authors contributed to the discussions and revisions.

COMPETING INTERESTS

The authors declare no competing interests.

ADDITIONAL INFORMATION

Correspondence and requests for materials should be addressed to D.L.

Reprints and permission information is available at http://www.nature.com/reprints

Publisher's note Springer Nature remains neutral with regard to jurisdictional claims in published maps and institutional affiliations.